2. EXPLANATORY NOTES[1]

Shipboard Scientific Party[2]

INTRODUCTION

In this chapter, we have assembled information that documents our scientific methods. This information concerns only shipboard methods described in the site reports in the *Initial Reports* volume of the Leg 165 *Proceedings of the Ocean Drilling Program* (ODP). Methods for shore-based analyses of Leg 165 data will be described in the individual scientific contributions to be published in the *Scientific Results* volume.

Coring techniques and core handling, including the numbering of sites, holes, cores, sections, and samples were the same as those reported in previous *Initial Reports* volumes of the *Proceedings of the Ocean Drilling Program* with two exceptions: The core sections from Holes 1002D and 1002E in the Cariaco Basin were not split during Leg 165; instead, they were transported to the Gulf Coast Repository (GCR) in College Station, Texas, so that they could be split, described, color scanned, and sampled under more controlled conditions. Also, Section 165-1001B-18R-5, which contained a Cretaceous/Tertiary boundary section, was taken to the GCR to be split with a nonferrous ceramic blade. This was done to reduce contamination and to minimize the loss of core during splitting. The other K/T boundary sections were taken to the GCR to be sampled. At the end of Leg 165, all other cores were transferred from the ship in refrigerated containers to cold storage in the ODP Core Repository in Bremen, Federal Republic of Germany, where the cores for Site 1002 and the K/T boundary cores will also eventually reside.

Authorship of Site Chapters

The separate sections of the site chapters were written by the following shipboard scientists (authors are listed in alphabetical order, with no seniority implied):

Site Summary: Leckie, Peterson, Sigurdsson
Background and Objectives: Droxler, Leckie, Peterson, Sigurdsson
Seismic Stratigraphy: Abrams, Cunningham, Droxler, Sigurdsson
Operations: Acton, Storms
Lithostratigraphy: Carey, Cotillon, Droxler, Gonzales, Haug, Mutti, Pearce, Peterson
Biostratigraphy: Bralower, Chaisson, D'Hondt, Kameo, Leckie
Paleomagnetism: Acton, Galbrun, King
Sedimentation and Mass Accumulation Rates: Acton, Bralower, Chaisson, King, Leckie, Murray
Igneous Petrology and Volcanology: Carey, Sigurdsson
Geochemistry: Lyons, Murray, Pearson, Sigurdsson
Physical Properties: Cunningham, Lind, Röhl
Downhole Measurements: Abrams, Louvel, Myers
Summary and Conclusions: Shipboard Scientific Party

[1]Sigurdsson, H., Leckie, R.M., Acton, G.D., et al., 1997. *Proc. ODP, Init. Repts.*, 165: College Station, TX (Ocean Drilling Program).
[2]Shipboard Scientific Party is given in the list preceding the Table of Contents.

Shipboard Scientific Procedures

Numbering of Sites, Holes, Cores, and Samples

Drilling sites are numbered consecutively from the first site drilled by the *Glomar Challenger* in 1968. A site number refers to one or more holes drilled while the ship was positioned over one acoustic beacon. Multiple holes may be drilled at a single site by pulling the drill pipe above the seafloor (out of the hole), moving the ship some distance from the previous hole, and then drilling another hole. In some cases, the ship may return to a previously occupied site to drill additional holes.

For all ODP drill sites, a letter suffix distinguishes each hole drilled at the same site. For example, the first hole drilled is assigned the site number modified by the suffix "A," the second hole takes the site number and suffix "B," and so forth. Note that this procedure differs slightly from the one used by Deep Sea Drilling Project (DSDP) (Sites 1–624), but prevents ambiguity between site- and hole-number designations. It is important to distinguish among holes drilled at a site, because recovered sediments or rocks from the same depth in different holes do not necessarily represent equivalent positions in the stratigraphic column.

The cored interval is measured in meters below seafloor (mbsf). The depth below seafloor is determined by subtracting the water depth estimated from the initial drill-pipe measurement (DPM), which gives the length of pipe from the rig floor to the seafloor, from the total DPM, which gives the length of pipe from the rig floor to the bottom of the hole (Fig. 1). Each cored interval is generally 9.5 m long, which is the length of a core barrel. Coring intervals may be shorter and may not necessarily be adjacent if separated by drilled intervals. In soft sediments, the drill string can be "washed ahead" with the core barrel in place without recovering sediments; this is achieved by pumping water down the pipe at high pressure to wash the sediment out of the way of the bit and up the annulus between the drill pipe and the wall of the hole. In drilling hard rock, a center bit may replace the core barrel if it is necessary to drill without core recovery.

Cores taken from a hole are numbered serially from the top of the hole downward. Core numbers and their associated cored intervals, in meters below seafloor (mbsf), usually are unique in a given hole; however, this may not be true if an interval must be cored twice, because of caving of cuttings or other hole problems. Maximum full recovery for a single core is 9.5 m of rock or sediment contained in a plastic liner (6.6-cm internal diameter) plus about 0.2 m (without a plastic liner) in the core catcher (Fig. 2). The core catcher is a device at the bottom of the core barrel that prevents the core from sliding out when the barrel is being retrieved from the hole. For sediments, the core-catcher sample is extruded into a short piece of plastic liner and is treated as a separate section below the last core section. For hard rocks, material recovered in the core catcher is included at the bottom of the last section. In certain situations (e.g., when coring gas-charged sediments that expand while being brought on deck), recovery may exceed the 9.5-m maximum.

A recovered core is divided into 1.5-m sections that are numbered serially from the top (Fig. 2). When full recovery is obtained, the sections are numbered from 1 through 7, with the last section possibly

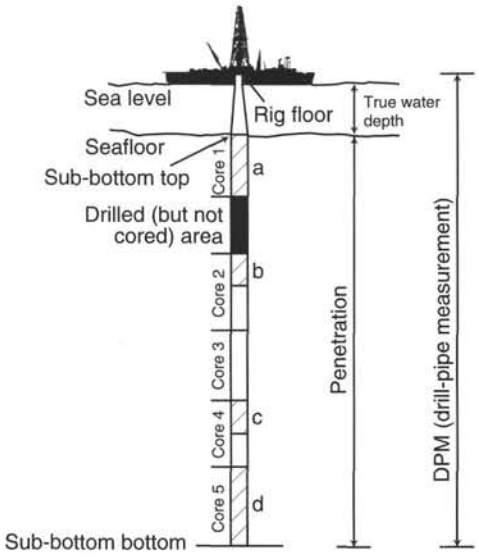

Represents recovered material

Bottom felt: distance from rig floor to seafloor

Total depth: distance from rig floor to bottom of hole (sub-bottom bottom)

Penetration: distance from seafloor to bottom of hole (sub-bottom bottom)

Number of cores: total of all cores recorded, including cores with no recovery

Total length of cored section: distance from sub-bottom top to sub-bottom bottom minus drilled (but not cored) areas in between

Total core recovered: total from adding a, b, c, and d in diagram

Core recovery (%): equals total core recovered divided by total length of cored section times 100

Figure 1. Terminology for coring and depth intervals.

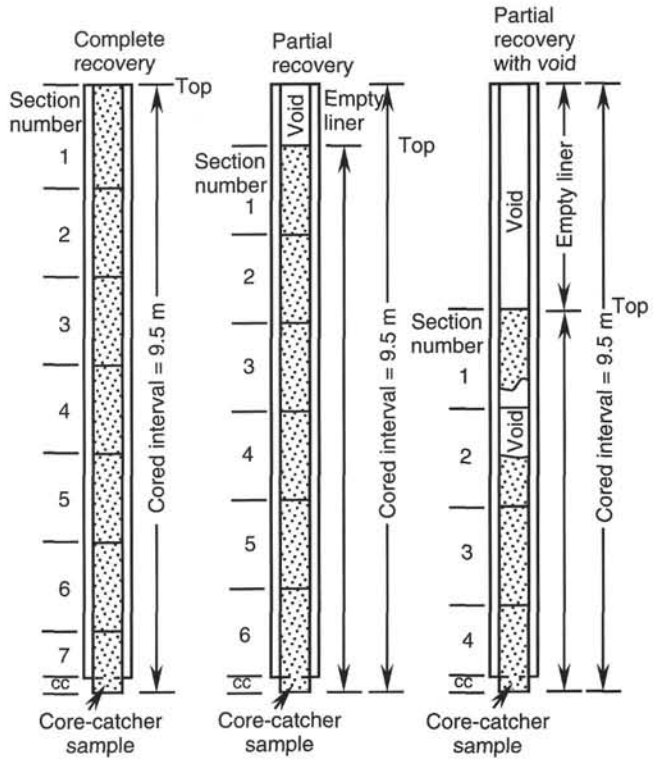

Figure 2. Examples of the numbering scheme for core sections.

being shorter than 1.5 m (rarely, an unusually long core may require more than seven sections). When less than full recovery is obtained, there will be as many sections as needed to accommodate the length of the core recovered; for example, 4 m of core would be divided into two 1.5-m sections and one 1-m section. If cores are fragmented (recovery less than 100%), sections are numbered serially and intervening sections are noted as void, whether shipboard scientists think that the fragments were contiguous in situ or not. In rare cases, a section less than 1.5 m may be cut to preserve features of interest, such as lithologic contacts.

By convention, material recovered from the core catcher of a sedimentary core is placed in a separate section during the core description, labeled core catcher (CC), and placed below the last section recovered in the liner. The core catcher is placed at the top of the cored interval in cases where material is only recovered in the core catcher. However, information supplied by the drillers or by other sources may allow for more precise interpretation as to the correct position of core-catcher material within an incompletely recovered cored interval.

When the recovered core is shorter than the cored interval, the top of the core is equated with the top of the cored interval, by convention to achieve consistency in handling analytical data derived from the cores. Samples removed from the cores are designated by distance measured in centimeters from the top of the section to the top and bottom of each sample removed from that section. In curated hard-rock sections, sturdy plastic spacers are placed between pieces that did not fit together to protect them from damage in transit and in storage. Therefore, the centimeter interval noted for a hard-rock sample gives only a physical reference to the location of the sample within the curated core.

A full identification number for a sample consists of the following information: leg, site, hole, core number, core type, section number, piece number (for hard rock), and interval in centimeters measured from the top of the section. For example, a sample identification of "165-998A-5H-1, 10–12 cm" would be interpreted as representing a sample removed from the interval between 10 and 12 cm below the top of Section 1, Core 5 (H designates that this core was taken during hydraulic piston coring) of Hole 998A during Leg 165.

All ODP core identifiers indicate core type. The following abbreviations are used: H = hydraulic piston corer (HPC; also referred to as APC, or advanced hydraulic piston corer), X = extended core barrel (XCB), R = rotary core barrel (RCB), N = motor-driven core barrel (MDCB, or "Navidrill"), P = pressure core sampler (PCS); V = vibra-percussive corer (VPC); B = drill-bit recovery; C = center-bit recovery; W = wash-core recovery; and M = miscellaneous material. On Leg 165, drilling was accomplished with the APC, XCB, and RCB drill bits only.

Core Handling

Sediments

As soon as a core is retrieved on deck, it goes through a sequence of processing steps (Fig. 3): First, a sample is taken from the core catcher and given to the paleontological laboratory for an initial age assessment. The core is then placed on the long horizontal rack, and gas samples are taken by piercing the core liner and withdrawing gas into a vacuum tube ("Vacutainer"). Voids within the core are sought as sites for gas sampling. Next, the core is marked into section lengths, each section is labeled, and the core is cut into sections. Interstitial-water (IW) whole-round samples are then taken as a matter of ODP policy (typically on every third core); whole-round samples for organic geochemistry may also be taken at this stage if they have been requested. Each section is then sealed at the top and bottom by gluing on color-coded plastic caps, blue to identify the top of a section and clear for the bottom. A yellow cap is placed on the section ends from which a whole-round sample has been removed, and the

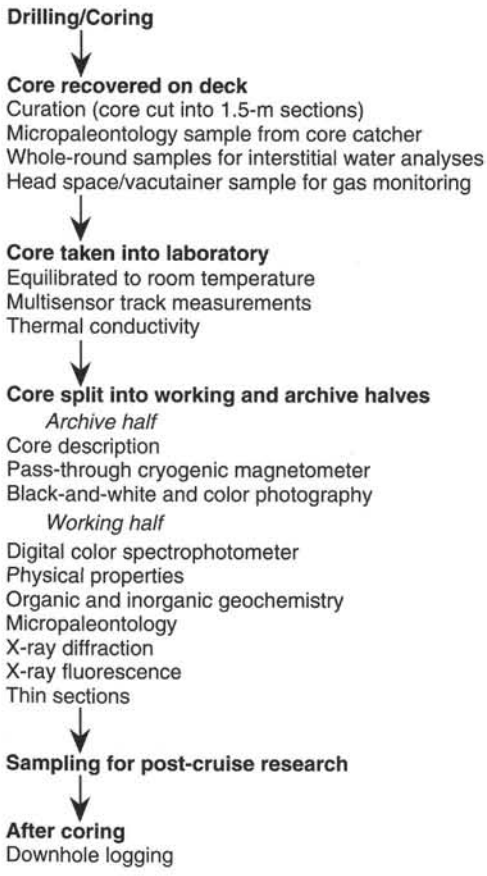

Figure 3. Generalized sequence of core flow and scientific data collection.

sample code (e.g., IW) is written on the yellow cap. The caps are usually attached to the liner by coating the end liner and the inside rim of the cap with acetone.

The core sections are then carried into the laboratory, where the individual sections are again labeled using an engraver to permanently mark the full designation of the section. The length of the core in each section and the core-catcher sample are measured to the nearest centimeter; this information is logged into the shipboard CORELOG database program.

Sections from APC and XCB cores are normally run through the multisensor track (MST) before splitting. The MST includes the GRAPE (gamma-ray attenuation porosity evaluator), *P*-wave logger devices (which measure bulk density, porosity, and sonic velocity) a susceptibility meter that measures the volume magnetic susceptibility, and a natural gamma radiation detector. At this point, whole-round samples for physical properties (PP) and structural analysis are taken. In well-lithified sedimentary cores, the core liner is split and the top half removed so that the whole-round core can be observed before choosing the samples. Relatively soft sedimentary cores are equilibrated to room temperature (approximately 3 hr) before thermal conductivity measurements are performed.

Cores of soft material are split lengthwise into working and archive halves. The softer cores are split with a wire or saw, depending on the degree of induration. Harder cores are split with a band or diamond saw. The wire-cut cores are split from the bottom to top, so investigators should be aware that older material could have been transported up the core on the split face of each section.

The working half of the core is sampled for both shipboard and shore-based laboratory studies. Each extracted sample is logged into the sampling computer database program by the location and the name of the investigator receiving the sample. Records of all removed samples are kept by the curator at ODP. The extracted samples are sealed in plastic vials or bags and labeled. Samples are routinely taken for shipboard physical properties analysis. These samples are subsequently used for calcium carbonate (coulometric analysis) and organic carbon (CNS elemental analyzer), and the data are reported in the site chapters.

The archive half is described visually. Smear slides are made from samples taken from the archive half and are supplemented by thin sections taken from the working half. Most archive sections are run through the cryogenic magnetometer. The archive half is then photographed with both black-and-white and color film, an entire core at a time. Close-up photographs (black-and-white) are taken of particular features for illustrations in the summary of each site, as requested by individual scientists. Both halves of the core are then put into labeled plastic tubes, sealed, and transferred to cold-storage space aboard the drilling vessel.

At the end of the leg, the cores were transferred from the ship in refrigerated airfreight containers to cold storage at the ODP Core Repository in Bremen, Federal Republic of Germany.

LITHOSTRATIGRAPHY

Sediment Core Description Forms

The sediment core description forms, or barrel sheets, summarize the data obtained during shipboard analysis of each core (Fig. 4). The ODP conventions used for compilation of each part of the core description forms and the exceptions to these procedures adopted by the Leg 165 Shipboard Scientific Party are described below.

Graphic Lithology Column

The lithological classification scheme of Mazzullo et al. (1988) was used in a slightly modified version on Leg 165. The classification adopted is outlined in the "Sediment Classification" section of this chapter. The only significant modification is a further subdivision of volcaniclastic sediment into fine ash and coarse ash. Sediment type is represented graphically on the core description forms using the symbols illustrated in Figure 5.

In the "Graphic Lithology" column, a maximum of three different lithologies (for interbedded sediments) or three different components (for mixed sediments) can be represented within the same core interval. Percentages are rounded to the nearest 10% and only lithologies that constitute at least 10% of the core are shown. Only lithologic units that are 20 cm or greater in thickness can be portrayed in this column. Minor lithologies present as thin interbeds within the major lithology are shown by a dashed vertical line dividing the lithologies. Components present as minor fractions of the main lithology are shown by a continuous vertical line.

Chronostratigraphy

The chronostratigraphic unit, based on paleontological results, is shown in the "Age" column. Zonations and ages used during Leg 165 are presented in the "Biostratigraphy" section of this chapter.

Sedimentary Structures

The location and nature of sedimentary structures in the cores is shown in the "Structure" column of the core description form. It is divided into three vertical areas for symbols. Typically, the intensity of bioturbation (slight, moderate, heavy) is shown in one column. Individual structures are shown in graphic form in either of the other "Structure" columns. The symbols used to designate the structures found in Leg 165 cores are shown in Figure 6.

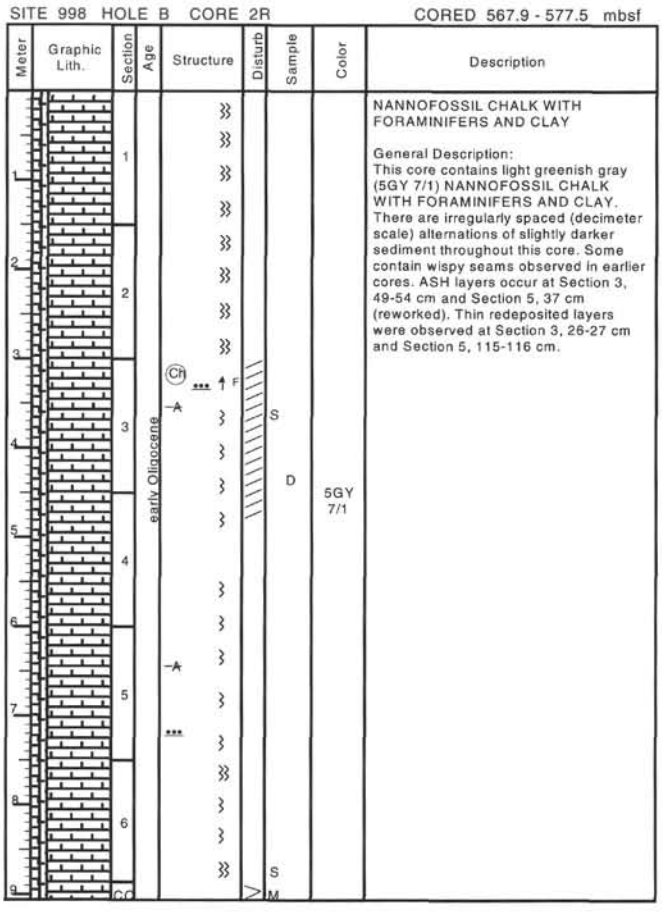

Figure 4. Example of core description form (barrel sheet) used for sediments and sedimentary rocks on Leg 165.

Sediment Disturbance

Observations of drilling-related disturbance over an interval of 20 cm or more are recorded in the "Disturbance" column using the symbols shown in Figure 6. The degree of drilling disturbance is described for soft and firm sediments using the following categories:

1. Slightly disturbed: bedding contacts are slightly deformed.
2. Moderately disturbed: bedding contacts have undergone extreme bowing.
3. Highly disturbed: bedding is completely deformed as flow-in, coring/drilling slough, and other soft sediment stretching and/or compressional shearing structures attributed to the coring/drilling.
4. Soupy: intervals are water-saturated and have lost all aspects of original bedding.

The degree of fracturing in indurated sediments and igneous rocks is described using the following categories:

1. Slightly fractured: core pieces are in place and broken.
2. Moderately fractured: core pieces are in place or partly displaced, and original orientation is preserved or recognizable (drilling slurry may surround fragments; i.e., drilling/coring "biscuits" are evident).
3. Highly fractured: core pieces are probably in correct stratigraphic sequence (although they may not represent the entire sequence), but original orientation is lost.
4. Drilling breccia: the core is crushed and broken into many small and angular pieces, with original orientation and stratigraphic position lost; often drilling breccia is completely mixed with drilling slurry.

Samples

The positions of samples taken for analysis from each core are indicated by letters in the "Sample" column of the core description form as follows: S (smear slide), T (thin section), M (micropaleontology), I (interstitial water), B (micropaleontology thin section), F (X-ray fluorescence geochemistry), and D (X-ray diffraction).

Color

Color, hue, and chroma attributes were determined after the core was split using a Minolta CM-2002 hand-held spectrophotometer. These measurements were made on the damp core surface, and clear plastic Saran wrap film was used to cover the core. The Minolta CM-2002 measures reflected visible light in 31, 10-nm-wide spectral bands ranging from 400 to 700 nm. These reflectance measurements were taken at 5-cm intervals for all cores. To correct the readings taken using plastic-film-covered cores, see Appendix A of the *Initial Reports* from Leg 154 (Shipboard Scientific Party, 1995).

Lithologic Description

The lithologic description that appears on each of the core description forms consists of a list of major lithologies followed by a more detailed description of the composition (as determined from smear slides), color, sedimentary features, and other notable features. Descriptions and locations of thin, interbedded, or minor lithologies are also included in the text. The terminology for the thickness of sedimentary beds and laminae follows McKee and Weir (1953): very thick bedded (>100 cm), thick bedded (30–100 cm), medium bedded (10–30 cm), thin bedded (3–10 cm), thickly laminated (>0.3 cm), and thinly laminated (<0.3 cm). The term "wispy lamination" was used to describe laminae observed at the sites that were undulatory and anastomosing in nature.

Additional data collected during Leg 165, such as grain size, wireline logs, paleomagnetic, geochemical, micropaleontological, and physical properties data, may be plotted as downcore profiles in the two columns to the left of the meter scale on the core description form (Fig. 4).

Smear Slide

Tables summarizing data from smear-slide and thin-section analyses are included on CD-ROM in the back pocket of this *Initial Reports* volume. These tables include information about the sample location, whether the sample represents a dominant (D) or a minor (M) lithology in the core, and the estimated percentages of sand, silt, and clay, together with all identified components.

X-ray Diffraction

Bulk-rock X-ray diffraction (XRD) analyses were undertaken on a limited number of samples to determine their mineral compositions. Standard XRD operating procedures and conditions were adhered to, and an interactive software package (R. Petschick, Macdiff 3.1, 1995) was used to help identify the main minerals and measure peak areas. Only qualitative estimates of mineral abundances were made; minor mineral inflections in the XRD peak profiles were designated as containing trace quantities (TR), and other observed components denoted as present (P). Peak area measurements of the clays were taken throughout the range from 4.4Å to 4.6Å, as most clays have vary-

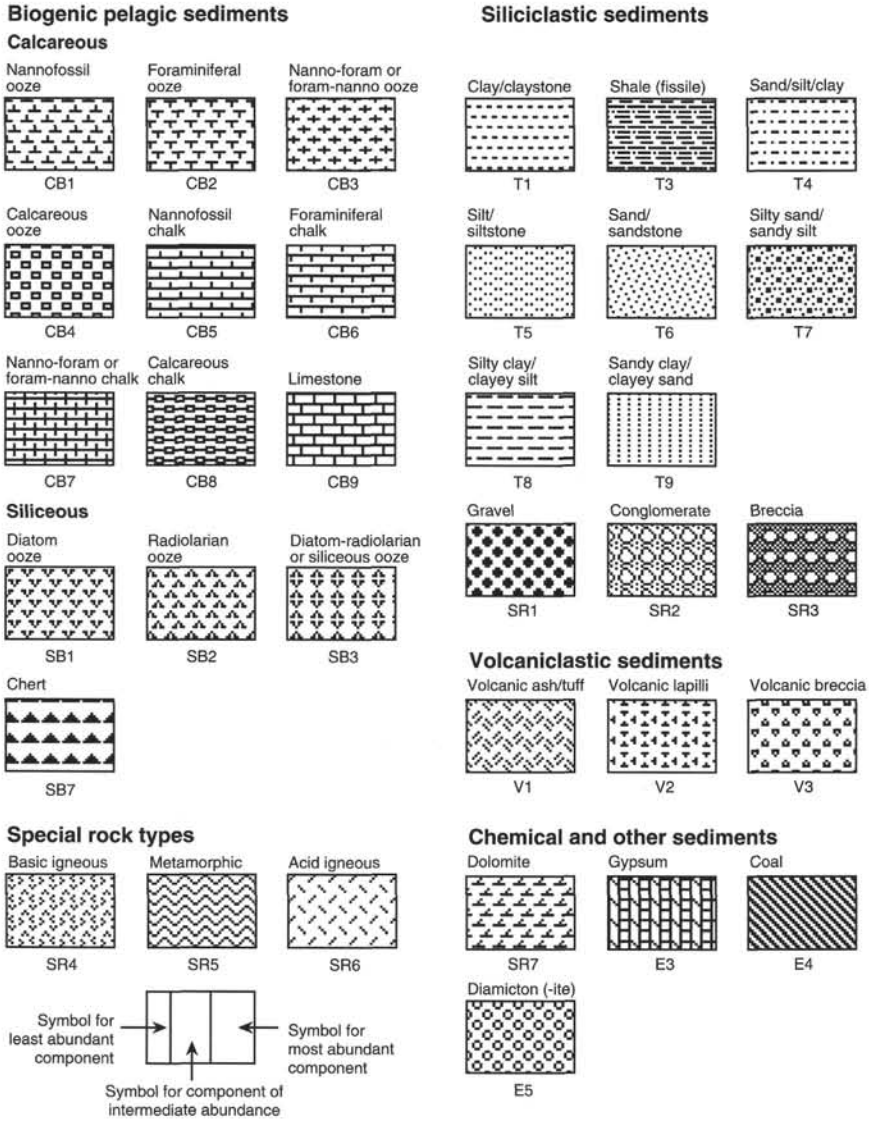

Figure 5. Key to symbols used in the "Graphic Lithology" column on the core description forms.

ing hkl (020, 111) diffractions at approximately 4.5Å. Quartz area measurements were taken from the hkl 101 peak at 3.42Å.

Sediment Classification

Classification of Sediments and Sedimentary Rocks

The slightly modified version of the sediment classification scheme of the ODP (Mazzullo et al., 1988) used on Leg 165 is described below. This classification scheme recognizes two principal sediment types: granular and chemical. Chemical sediments were not encountered during Leg 165.

Classes of Granular Sediments

Variations in the relative proportions of different grain types define five major classes of granular sediments: pelagic, neritic, siliciclastic, volcaniclastic, and mixed (Fig. 7). Pelagic grains are the skeletal remains of open-marine siliceous and calcareous microbiota (e.g., radiolarians, diatoms, planktonic foraminifers, nannofossils) and associated organisms. Neritic grains include calcareous grains and skeletal remains (e.g., bioclasts, shallow-water benthic foraminifers, peloids) of nonpelagic origin. Inorganic and organic fine-grained (fine silt to clay size) metastable carbonate particles (aragonite and magnesian calcite), produced on the top of carbonate banks, transported offshore, mixed with the pelagic grains, and deposited on the seafloor by settling through the water column, are referred to as micrite (sensu lato). Siliciclastic grains are mineral and rock fragments derived from plutonic, sedimentary, and metamorphic rocks. Volcaniclastic grains include those of pyroclastic (direct products of magma degassing) and epiclastic origin (detritus derived from erosion of volcanic rocks).

Classification of Granular Sediment

A granular sediment is classified by designating a principal name with additional major and minor modifiers. The principal name of a granular sediment defines its granular-sediment class. The major and minor modifiers describe the texture, composition, fabric, or roundness of the grains themselves.

Each granular-sediment class has a unique set of principal names. A summary of these principal names is presented in Table 1. For a complete discussion see Mazzullo et al. (1988). We modified slightly the classification of Mazzullo et al. (1988) in regard to principal names of volcaniclastic sediments. Volcaniclastic sediments have been divided into two groups: pyroclastic and epiclastic. The names and ranges of three size groups for pyroclastic material (from Fisher and Schmincke, 1984) are as follows:

1. *Volcanic breccia:* clasts >64 mm in diameter;

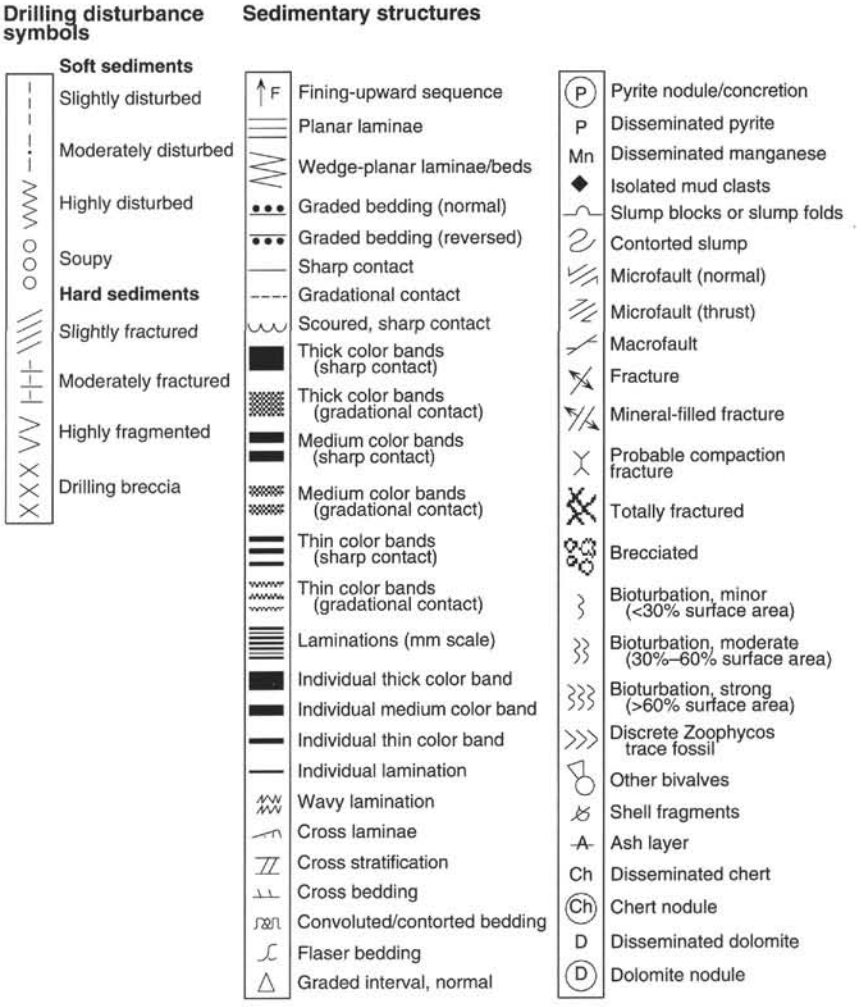

Figure 6. Symbols used for drilling disturbance and sedimentary structures on core description forms.

2. *Lapilli:* clasts between 2 and 64 mm in diameter; described as lapillistone when lithified; and
3. *Ash:* grains <2 mm in diameter, described as tuff when lithified.

We further divided the ash component of the ODP scheme into two size classes: material ranging from 63 µm to 2 mm in grain size (equivalent to sand in siliciclastic sediments) is described as *coarse ash,* and material less than 63 µm (silt and clay-size) is termed *fine ash.* Coarse tuff and fine tuff are the terms used for lithified equivalents of these size ranges. For epiclastic sediments, the principal name is based on grain size using the same nomenclature as in the classification for siliciclastic sediments (Udden-Wentworth grain size scale).

Major and Minor Modifiers

The principal name of a granular-sediment class is preceded by major modifiers and followed by minor modifiers (preceded by "with") that describe the lithology of the granular sediment in greater detail (Table 1). Major and minor modifiers are used most commonly to describe composition and grain size of particles present in major (>25%) and minor (10%–25%) proportions. In addition, major modifiers can be used to describe degree of lithification, grain fabric, grain shape, and sediment color. Note that the major modifiers are always listed in order of increasing abundance. As an example, an unconsolidated pelagic sediment containing 30% clay, 15% foraminifers, and 55% nannofossils is called a clayey nannofossil ooze with foraminifers. Also an ooze, chalk, or limestone deposited in the vicinity of shallow carbonate banks, with the term micrite (sensu lato) as either a major or minor modifier, was also referred to in the text as

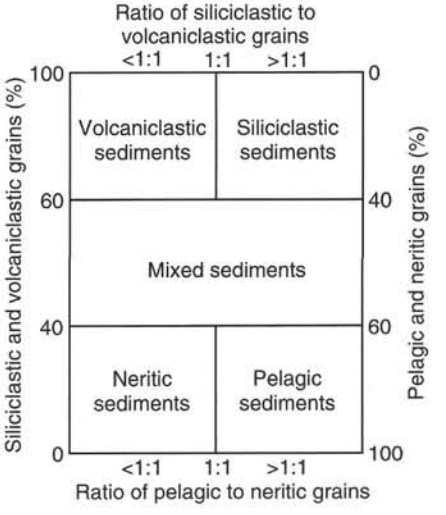

Figure 7. Diagram showing classes of granular sediment (after Mazzullo et al., 1988).

periplatform ooze, chalk, or limestone, as defined by Schlager and James (1978).

The principal modifiers used in the classification of volcaniclastic sediments include lithic (rock fragments), vitric (glass, pumice, or hyaloclastite), crystal (mineral crystals and fragments), and modifiers describing the composition of the lithic grains and crystals (e.g., feld-

Table 1. Outline of granular-sediment classification scheme.

Sediment class	Major modifiers	Principal name	Minor modifiers
Pelagic sediment	1. Composition of pelagic and neritic grains present in major amounts 2. Texture of clastic grains present in major amounts	1. Ooze 2. Chalk 3. Limestone 4. Radiolarite 5. Diatomite 6. Spiculite 7. Chert	1. Composition of pelagic and neritic grains present in minor amounts 2. Texture of clastic grains present in minor amounts
Neritic sediment	1. Composition of neritic and pelagic grains present in major amounts 2. Texture of clastic grains present in major amounts	1. Boundstone 2. Grainstone 3. Packstone 4. Wackestone 5. Mudstone 6. Floatstone 7. Rudstone	1. Composition of neritic and pelagic grains present in minor amounts 2. Texture of clastic grains present in minor amounts
Siliciclastic sediment	1. Composition of all grains present in major amounts 2. Grain fabric (gravels only) 3. Sediment color (optional) 4. Grain shape (optional)	1. Gravel 2. Sand 3. Silt 4. Clay	1. Composition of all grains present in minor amounts 2. Texture and composition of siliciclastic grains present as matrix (for coarse-grained clastic sediments)
Volcaniclastic sediments	1. Composition of all volcaniclasts present in major amounts 2. Composition of all pelagic and neritic grains present in major amounts 3. Texture of siliciclastic grains present in major amounts	1. Breccia 2. Lapilli 3. Ash/tuff	1. Composition of all volcaniclasts present in minor amounts 2. Composition of all pelagic and neritic grains present in minor amounts 3. Texture of siliciclastic grains present in minor amounts
Mixed sediments	1. Composition of neritic and pelagic grains present in major amounts 2. Texture of clastic grains present in major amounts	1. Mixed sediments	1. Composition of neritic and pelagic grains present in minor amounts 2. Texture of clastic grains present in minor amounts

Note: Scheme has been modified from Mazzullo et al. (1988).

spar or basaltic). For a complete discussion of the nomenclature for major and minor modifiers, see Mazzullo et al. (1988).

BIOSTRATIGRAPHY

Introduction

Preliminary age assignments were based on biostratigraphic analyses of calcareous nannofossils and planktonic foraminifers. Stratigraphic constraint of calcareous nannofossil datums was achieved by examining one sample per section of core (a sample spacing of 1.5 m). Planktonic foraminifer datums were initially located by examination of sediments from core catchers, and in places further constrained by examination of one to two samples per 9.5 m core. Hole-to-hole correlations were achieved by selecting biostratigraphic datums that are thought to be isochronous.

The relative abundance, preservation, and zonal assignment for each sample are recorded in the FossiList database.

All age estimates of biostratigraphic data were calibrated to the updated magnetic polarity time scale of Cande and Kent (1995) (Tables 2, 3; Fig. 8). Age estimates of planktonic foraminifer and nannofossil datums between 0 and 5 Ma are equivalent to those of Curry, Shackleton, Richter, et al. (1995). In this time scale, ages of datums lying between magnetic anomalies were dated with orbitally tuned time scales of Shackleton et al. (1995) and Hilgen (1991a, 1991b). Age estimates of nannofossil datums between 5 and 14 Ma were taken from the orbitally tuned estimates of Backman and Raffi (in press). Age estimates of most planktonic foraminifer datums between 5 and 65 Ma, and most nannofossil datums between 14 and 65 Ma were taken from Berggren et al. (1995) (Fig. 8). Causes of uncertainty about the age estimates for older intervals include variation in accumulation rates between magnetic reversals, sample spacing in the stratigraphic studies used to construct the time scales, and radiometric dating uncertainties. A second significant digit is appended to the absolute age estimates for datums within Zone P0 (Table 3). This convention is adopted to show that the events occur *within* this brief period (~0.10 Ma), rather than at the lower or upper boundary, and that the second digit has no bearing on the actual precision of the age estimates.

The time scale of Gradstein et al. (1994) was applied in the Cretaceous. Age estimates for most Late Cretaceous planktonic foraminifer and nannofossil datums were taken from the compilation of Erba et al. (1995), which is based on the time scale of Gradstein et al. (1994) (Fig. 8). We noted, however, a few discrepancies within this scheme (see Bralower and Siesser [1992] for a synthesis of biomagnetostratigraphic correlation). These include the following: the first occurrence (FO) of *Micula prinsii* correlates with Subchron C29r instead of Subchron C30n; the FO of *Nephrolithus frequens* and *Micula murus* correlate with Subchron C30n instead of Subchrons C31n and C31r, respectively; and the last occurrence (LO) of *Tranolithus orionatus phacelosus* correlates with Subchron C31r instead of Subchron C32n. In addition, the LO of *Eprolithus floralis* lies in the lower instead of the upper Santonian. In these cases, we calibrated age estimates of datums from Bralower et al. (1995) and Bralower et al. (unpubl. data) to the Gradstein et al. (1994) time scale. Few nannofossil and planktonic foraminifer events lie at stage boundaries or close to radiometric age estimates. Thus, considerable error occurs in using these datums for sedimentation rate estimates and chronostratigraphy. Particularly large errors exist in the definition of the Campanian/Maastrichtian boundary as well as the upper and lower boundaries of the Coniacian stage. For example, the former boundary had previously been placed at the top of the *Globotruncanita calcarata* planktonic foraminifer Zone (e.g., Sigal, 1977; Caron, 1985), but it has been reassigned recently to the middle *Gansserina gansseri* zone by Premoli Silva and Sliter (1994) based on studies of northern European sections.

Calcareous Nannofossils

During Leg 165, we applied the zonal scheme of Bukry (1973, 1975; code numbers of Okada and Bukry, 1980) for the Cenozoic. This zonation, compiled from a study of Caribbean sequences on DSDP Leg 15, is regarded as a general framework for the biostratigraphic classification of low-latitude Cenozoic marine sediments based on calcareous nannofossils. For the Cretaceous, we use the zonation scheme of Sissingh (1977), with one minor modification: because of the difficulty in distinguishing species of *Reinhardtites* in

Table 2. Age estimates of calcareous nannofossil datum events.

Event	Zone (base)	Age (Ma)	Reference
B Acme *Emiliania huxleyi*		0.085	1
T *Helicosphaera inversa*		0.155	2
B *Emiliania huxleyi*	CN15	0.248	2
T *Pseudoemiliania lacunosa*	CN14b	0.408	2
B *Helicosphaera inversa*		0.505	2
T *Reticulofenestra asanoi*		0.88	3
B *Gephyrocapsa parallela*	CN14a	0.94	3
B *Reticulofenestra asanoi*		1.17	3
T Large *Gephyrocapsa* spp.		1.23	3
T *Helicosphaera sellii*		1.26	3
B Large *Gephyrocapsa* spp.		1.48	3
T *Calcidiscus macintyrei*		1.64	3
B *Gephyrocapsa oceanica*		1.64	3
B *Gephyrocapsa caribbeanica*	CN13b	1.71	4
Pliocene/Pleistocene boundary		1.745	2
T *Discoaster brouweri*	CN13a	1.95	3
T *Discoaster pentaradiatus*	CN12d	2.36	3
T *Discoaster surculus*	CN12c	2.51	3
T *Discoaster tamalis*	CN12b	2.82	2
T *Sphenolithus* spp.	CN12a	3.62	5
T *Reticulofenestra pseudoumbilicus*	CN12a	3.83	3
T *Amaurolithus* spp.	CN11	4.50	6
B *Ceratolithus rugosus*	CN10c	5.046	7
B *Ceratolithus acutus*	CN10b	5.089	7
T *Triquetrorhabdulus rugosus*		5.231	7
Miocene/Pliocene boundary		5.3	
T *Discoaster quinqueramus*	CN10a	5.537	7
B *Amaurolithus* spp.	CN9b	7.392	7
B *Discoaster berggrenii*	CN9a	8.281	7
B *Discoaster loeblichii*	CN8b	8.7	8
T *Discoaster hamatus*	CN8a	9.635	7
B *Discoaster neohamatus*		10.450	7
B *Discoaster hamatus*	CN7	10.476	7
B *Catinaster coalitus*	CN6	10.794	7
T *Coccolithus miopelagicus*		10.941	7
T *Discoaster kugleri*		11.520	7
B *Discoaster kugleri*	CN5b	11.831	7
T *Cyclicargolithus floridanus*		13.2	9
T *Sphenolithus heteromorphus*	CN5a	13.523	7
T *Helicosphaera ampliaperta*	CN4	15.6	8
T Abundant *Discoaster deflandrei*		16.2	9
B *Sphenolithus heteromorphus*	CN3	18.2	8
T *Sphenolithus belemnos*		18.3	8
B *Sphenolithus belemnos*	CN2	19.2	8
B *Discoaster druggii*	CN1c	23.3	11
Oligocene/Miocene boundary		23.8	
T *Sphenolithus delphix*		23.8	8
T *Reticulofenestra bisecta*	CN1a	23.9	8
T *Zygrhablithus bijugatus*		24.5	8
T *Sphenolithus ciperoensis*		25.5	8
T *Sphenolithus distentus*	CP19b	27.5	8
B *Sphenolithus ciperoensis*	CP19a	29.9	8
B *Sphenolithus distentus*	CP18	31.5	8
T *Reticulofenestra umbilicus*	CP17	32.3	8
T *Ericsonia formosa*	CP16c	32.8	8
T Acme *Ericsonia subdisticha*	CP16b	33.3	8
Eocene/Oligocene boundary		33.7	
T *Discoaster saipanensis*	CP16a	34.2	8
T *Discoaster barbadiensis*	CP16a	34.3	8
T *Cribrocentrum reticulatum*		35.0	8
T *Chiasmolithus grandis*	CP15	37.1	8
B *Reticulofenestra bisecta*		38.0	8
T *Chiasmolithus solitus*	CP14b	40.4	8
B *Cribrocentrum reticulatum*		42.0	8
T *Nannotetrina fulgens*		43.1	8
B *Reticulofenestra umbilicus*	CP14a	43.7	8
T *Chiasmolithus gigas*	CP13c	44.5	8
B *Chiasmolithus gigas*	CP13b	46.1	8
B *Nannotetrina fulgens*	CP13a	47.3	8
B *Discoaster sublodoensis*	CP12	49.7	8
T *Tribrachiatus orthostylus*		50.6	8
B *Coccolithus crassus*	CP11	51.5	12
B *Discoaster lodoensis*	CP10	52.0	8
T *Tribrachiatus contortus*	CP9a	53.6	8
B *Tribrachiatus orthostylus*		53.6	8
Paleocene/Eocene boundary		54.7	
B *Tribrachiatus contortus*		54.7	12
B *Discoaster diastypus*	CP9a	55.0	12
B *Tribrachiatus bramlettei*	CP9a	55.0	8
T *Fasciculithus tympaniformis*		55.3	8
B *Discoaster multiradiatus*	CP8a	56.2	8
B *Discoaster nobilis*	CP7	56.9	8
B *Discoaster mohleri*	CP6	57.5	8
B *Heliolithus kleinpellii*	CP5	58.4	8
B *Fasciculithus tympaniformis*	CP4	59.7	8
B *Sphenolithus primus*		60.6	8
B *Ellipsolithus macellus*	CP3	62.2	8
B *Sullivanica danica*	CP2	63.8	8
B *Cruciplacolithus tenuis*	CP1b	64.5	8
B *Cruciplacolithus primus*		64.8	8
B *Biantholithus sparsus*		65.0	8
T Cretaceous taxa	CP1a	65.0	8
Cretaceous/Tertiary boundary		65.0	
B *Micula prinsii*		65.4	13
B *Nephrolithus frequens*	CC26	65.8	13
B *Micula murus*		66.2	13
B *Lithraphidites quadratus*		67.5	13
T *Reinhardities levis*	CC25	69.2	14
T *Tranolithus orionatus*	CC24	69.6	13
T *Quadrum trifidum*		71.3	14
T *Aspidolithus parcus*		74.5	14
T *Eiffellithus eximius*	CC23*	75.0	14
B *Quadrum trifidum*	CC22	76.0	14
B *Quadrum gothicum*	CC21	77.0	14
B *Ceratolithoides aculeus*	CC20	78.5	14

Notes: B = base, T = top. An asterisk (*) indicates that an alternate marker has been substituted for the original definition. References are as follows: 1 = Thierstein et al. (1977); 2 = modified from Takayama and Sato (1987), Sato et al. (1991), Takayama (1993), and Kameo et al. (1995); 3 = Wei (1993); 4 = Berger et al. (1994); 5 = Backman and Shackleton (1983); 6 = Backman et al. (1990); 7 = Backman and Raffi (in press); 8 = Berggren et al. (1995); 9 = Raffi and Flores (1995); 10 = Olafsson (1991); 11 = Berggren et al. (1985a, 1985b); 12 = modified from Curry, Shackleton, Richter, et al. (1995); 13 = modified from Bralower et al. (1995); 14 = Erba et al. (1996).

poorly preserved material, we substitute the LO of *Eiffellithus eximius* for the LO of *R. anthophorus* in order to define the base of Zone CC23 (see Bralower and Siesser, 1992). Bukry's (1973, 1975) Cenozoic and Sissingh's (1977) Cretaceous zonal schemes are presented in Figure 8 together with the geomagnetic polarity time scale (see "Paleomagnetism" section, this chapter).

Cenozoic biostratigraphic events, including Okada and Bukry's (1980) zonal indicators, are listed in Table 2. The events have been tied directly to magnetostratigraphic records, many of which are derived from extra-tropical environments. This is particularly true for the Paleogene events. In cases where Bukry used two datum events for definition of a given zonal/subzonal boundary, we have attempted to choose the datum that is more easily determined. A few of Bukry's (1973, 1975) subzones are not accounted for in Table 2. This generally indicates events that we consider time transgressive or difficult to determine due to extreme rarity of markers. Except where otherwise noted, we followed taxonomic concepts summarized in Aubry (1984, 1988, 1989, 1990) and Perch-Nielsen (1985a, 1985b).

Methods

Standard smear slides were made of all soft lithologies. Smear slides of indurated lithologies were prepared using the technique of Monechi and Thierstein (1985). Calcareous nannofossils were examined by means of standard light microscope techniques, under crossed nicols and transmitted light at ×1000 magnification.

We have adopted a simple system to characterize preservational states:

G = good (little or no evidence of dissolution and/or secondary overgrowth of calcite; diagnostic characters fully preserved);
M = moderate (dissolution and/or secondary overgrowth; partially altered primary morphological characteristics; however, nearly all specimens can be identified at the species level); and
P = poor (severe dissolution, fragmentation, and/or secondary overgrowth with primary features largely destroyed; many specimens cannot be identified at the species level and/or generic level).

Table 3. Age estimates of planktonic foraminifer datum events.

Event	Zone (base)	Age (Ma)	Reference
LO *Globigerinoides obliquus*		1.3	4
LO *Globigerinoides fistulosus*		1.7	1
Pliocene/Pleistocene boundary		1.745	
LO *Globigerinoides extremus*		1.9	1
FO *Globorotalia (Truncorotalia) truncatulinoides*	N22	2.0	1
LO *Globorotalia (Menardella) exilis*		2.2	1
LO *Globorotalia (Menardella) miocenica*		2.3	1
Reappearance of *Pulleniatina* (Atlantic)		2.3	1
LO *Globorotalia (Menardella) limbata*		2.4	4
LO *Globorotalia (Menardella) pertenuis*		2.6	1
LO *Dentoglobigerina altispira*		3.0	2
LO *Globorotalia (Menardella) multicamerata*		3.0	1
FO *Globorotalia (Truncorotalia) tosaensis*	N21	3.2	1
FO *Globigerinoides fistulosus*		3.2	1
FO *Globorotalia (Menardella) pertenuis*		3.5	1
LO *Pulleniatina* (Atlantic)		3.5	1
FO *Globorotalia (Menardella) miocenica*	N20	3.6	1
LO *Globorotalia (Hirsutella) margaritae*		3.6	1, 3
Δ *Pulleniatina* (S to D coiling change)		4.0	1, 2
LO *Globoturborotalita nepenthes*		4.3	1
LO *Globorotalia plesiotumida*		4.4	1
FO *Globorotalia (Menardella) exilis*		4.5	4
FO *Globorotalia (Truncorotalia) crassaformis* s.l.		4.7	1
LO *Globorotalia (Hirsutella) cibaoensis*		5.0	1, 2
Miocene/Pliocene boundary		5.3	3
LO *Globoquadrina baroemoenensis*		5.4	1
FO *Sphaeroidinella dehiscens* s.s.	N19	5.6	1
FO *Globorotalia tumida*	N18	5.9	1
FO *Globorotalia (Hirsutella) margaritae*		6.0	3
FO *Globigerinoides conglobatus*		6.2	4
? *Neogloboquadrina acostaensis* (D to S)		6.6	3
LO Sinistral *menardiform globorotaliids*		7.4	3
FO *Globorotalia (Hirsutella) cibaoensis*		7.7	1, 2
FO *Candeina nitida*		8.0	1, 2
FO *Globigerinoides extremus*		8.0	1, 2
FO *Globorotalia (Hirsutella) juanai*		8.0	1, 2
FO *Globorotalia plesiotumida*	N17	8.2	1
FO *Neogloboquadrina humerosa*		8.5	3
FO *Neogloboquadrina acostaensis*	N16	10.0	1
LO *Paragloborotalia mayeri*	N15	10.3	1
FO *Globorotalia (Menardella) limbata*		10.6	4
FO *Globoturborotalita apertura*		10.8	1, 2
FO *Globoturborotalita decoraperta*		11.2	1, 2
FO *Globoturborotalita nepenthes*	N14	11.4	1
LO *Fohsella fohsi* s.l.	N13	11.8	1
FO *Globorotalia lenguaensis*		12.3	1, 2
FO *Fohsella fohsi robusta*		12.3	3
FO *Fohsella fohsi* s.l.	N12	12.7	3
FO *Fohsella praefohsi*	N11	14.0	1
LO *Fohsella peripheroronda*		14.6	3
FO *Fohsella peripheroacuta*	N10	14.8	3
FO *Globorotalia (Menardella) praemenardii*		14.9	1, 2
FO *Orbulina* spp.	N9	15.1	3
FO *Globorotalia (Menardella) archeomenardii*		15.5	1, 2
FO *Praeorbulina circularis*		16.0	3
FO *Praeorbulina glomerosa*		16.1	3
FO *Praeorbulina sicana*	N8	16.4	3
LO *Catapsydrax dissimilis*	N7	17.3	3
FO *Globigerinatella insueta*	N6	18.8	3
LO *Globoquadrina binaiensis*		19.1	1, 2
LO *Globigerinoides altiapertura*		20.5	3
LO *Paragloborotalia kugleri*	N5	21.5	3
LO *Globoturborotalita angulisuturalis*		21.6	3
LO *Paragloborotalia pseudokugleri*		21.6	3
FO *Globoquadrina binaiensis*		22.1	1, 2
FO *Paragloborotalia kugleri*	N4	23.8	3
Oligocene/Miocene boundary		23.8	
FO *Globigerina euapertura*		23.8	3
FO *Globigerinoides primordius* (common)		24.3	3
FO *Paragloborotalia pseudokugleri*		25.9	3
FO *Globigerinoides primordius*		26.7	3
LO *Paragloborotalia opima*	P22	27.1	3
LO *Ch. cubensis* (common)	P21b	28.5	3
FO *Globoturborotalita angulisuturalis*	P21a	29.4	3
LO *Subbotina angiporoides*		30.0	3
LO *Turborotalia ampliapertura*	P20	30.3	3
FO *Paragloborotalia opima*		30.6	3
LO *Pseudohastigerina* spp.	P19	32.0	3
LO *Hantkenina* spp.		33.7	3
Eocene/Oligocene boundary		33.7	
LO *Turborotalia cerroazulensis*	P18	33.8	3
LO *Cribrohantkenina inflata*	P17	34.0	3
LO *Globogerapsis index*		34.3	3
FO *Turborotalia cunialensis*	P16	35.2	3

Table 3 (continued).

Event	Zone (base)	Age (Ma)	Reference
LO *Turborotalia pomeroli*		35.3	3
LO *Porticulasphaera semiinvoluta*		35.3	3
FO *Cribrohantkenina inflata*		35.5	3
LO *Acarinina collactea*		37.7	3
LO *Subbotina linaperta*		37.7	3
LO *Morozovella spinulosa*		38.1	3
FO *Porticulasphaera semiinvoluta*	P15	38.4	3
LO *Planorotalites*		38.5	3
LO *Acarinina* spp.		37.5–38.5	3
LO *Acarinina primitiva*		39.0	3
LO *Subbotina frontosa*		39.3	3
LO *Globigerapsis beckmanni*	P14	40.1	3
FO *Globogerapsis beckmanni*	P13	40.5	3
LO *Acarinina bullbrooki*		40.5	3
FO *Turborotalia pomeroli*		42.4	3
FO *Globigerapsis index*		42.9	3
FO *Morozovella lehneri*		43.5	3
LO *Morozovella aragonensis*	P12	43.6	3
FO *Globigerapsis kugleri*	P11	45.8	3
FO *Turborotalia possagnoensis*		46.0	3
FO *Hantkenina nuttali*	P10	49.0	3
FO *Planorotalites palmerae*	P9	50.4	3
LO *Morozovella formosa*	P8	50.8	3
FO *Acarinina pentacamerata*		50.8	3
FO *Morozovella aragonensis*	P7	52.3	3
LO *Morozovella marginodentata*		52.5	3
LO *Morozovella lensiformis*		52.7	3
LO *Subbotina velascoensis*		53.5	3
LO *Morozovella aequa*		53.6	3
FO *Morozovella formosa*	P6b	54.0	3
FO *Morozovella lensiformis*		54.0	3
LO *Morozovella velascoensis*	P6a	54.7	3
Paleocene/Eocene boundary		54.7	
LO *Morozovella acuta*		54.7	3
FO *Morozovella gracilis*		54.7(54.9)	3(5)
FO *Igorina broedermanni*		54.7	3
FO *Morozovella marginodentata*		54.8	3
FO *Morozovella subbotinae*		55.9	3
LO *Globanomalina pseudomenardii*	P5	55.9	3
LO *Acarinina nitida* (= *A. acarinata*)		56.3	3
LO *Acarinina mckannai*		56.3	3
FO *Acarinina soldadoensis*	P4c	56.5	3
FO *Acarinina coalingensis* (= *triplex*)		56.5	3
FO *Morozovella aequa*		56.5	3
LO *Acarinina subsphaerica*	P4b	57.1	3
FO *Acarinina mckannai*		59.1	3
FO *Acarinina subsphaerica*		59.2	3
FO *Acarinina nitida*		59.2	3
FO *Globanomalina pseudomenardii*	P4a	59.2	3
FO *Subbotina velascoensis*		~59.2	5
LO *Parasubbotina variospira*		59.2	5
FO *Morozovella velascoensis*		60.0	3
FO *Igorina albeari*	P3b	60.0	3
FO *Morozovella conicotruncata*		60.9	3
FO *Morozovella angulata*	P3a	61.0	3
FO *Igorina pusilla*		61.0	3
FO *Praemurica uncinata*	P2	61.2	3
FO *Globanomalina compressa*	P1c	63.0	3
FO *Praemurica inconstans*		63.0	3
FO *Parasubbotina varianta*		63.0	3
FO *Subbotina triloculinoides*	P1b	64.3	3
LO *Parvularugoglobigerina eugubina*	P1a	64.7(64.9)	3(5)
FO *Parvularugoglobigerina eugubina*	Pa	64.97	3
FO *Globoconusa daubjergensis*		64.97	3
FO *Woodringina claytonensis*		64.97	3
LO Most Cretaceous taxa	P0	65.0	3
Cretaceous/Tertiary boundary		65.0	3
FO *Abathomphalus mayaroensis*	*A. mayaroensis*	68.25	6
FO *Racemiguembelina fructicosa*		69.6	6
FO *Contusotruncana contusa*		69.6	6
FO *Gansserina gansseri*	*G. gansseri*	72.8	6
FO *Globotruncana aegyptiaca*	*G. aegypticaa*	73.8	6
LO *Globotruncanita calcarata*	*G. havanensis*	75.2	6
FO *Globotruncanita calcarata*	*G. calcarata*	75.7	6
FO *Globotruncana ventricosa*	*G. ventricosa*	79.5	6
FO *Rotalipora apenninica*	*R. apenninica*	100.4	6
FO *Rotalipora ticinensis*	*R. ticinensis*	101.8	6
FO *Rotalipora subticinensis*		102.5	6
FO *Biticinella breggiensis*	*B. breggiensis*	105.0	6

Notes: References are as follows: 1 = Curry, Shackleton, Richter, et al. (1995), after Berggren et al. (1985a, 1985b); 2 = Chaisson and Leckie (1993); 3 = Berggren et al. (1995); 4 = Chaisson and Pearson (in press); 5 = Paleogene Working Group on Planktonic Foraminifers (in press); 6 = Erba et al. (1996).

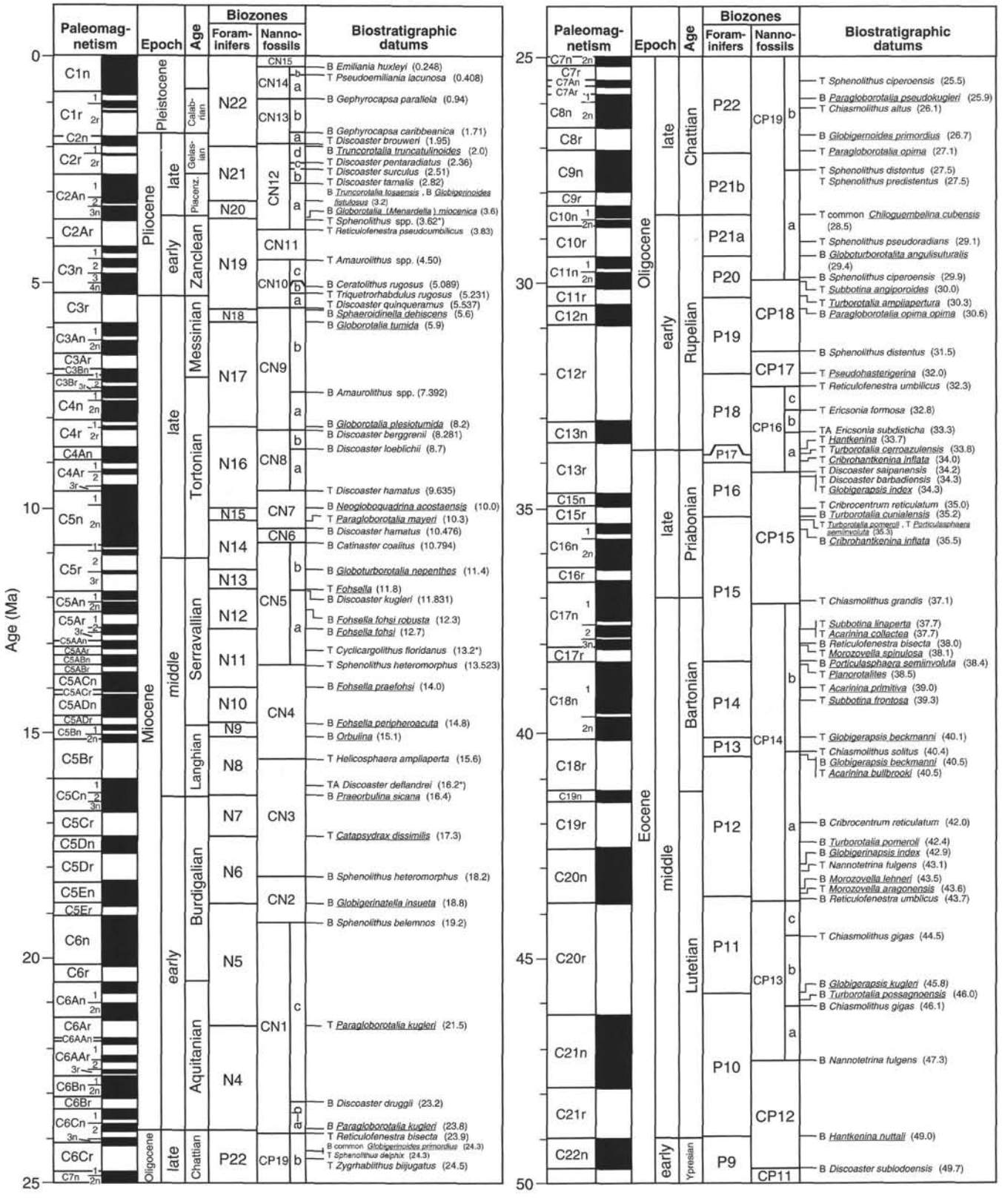

Figure 8. Correlation chart of nannofossil and planktonic foraminifer (underlined) datums for the interval from 0 to 80 Ma.

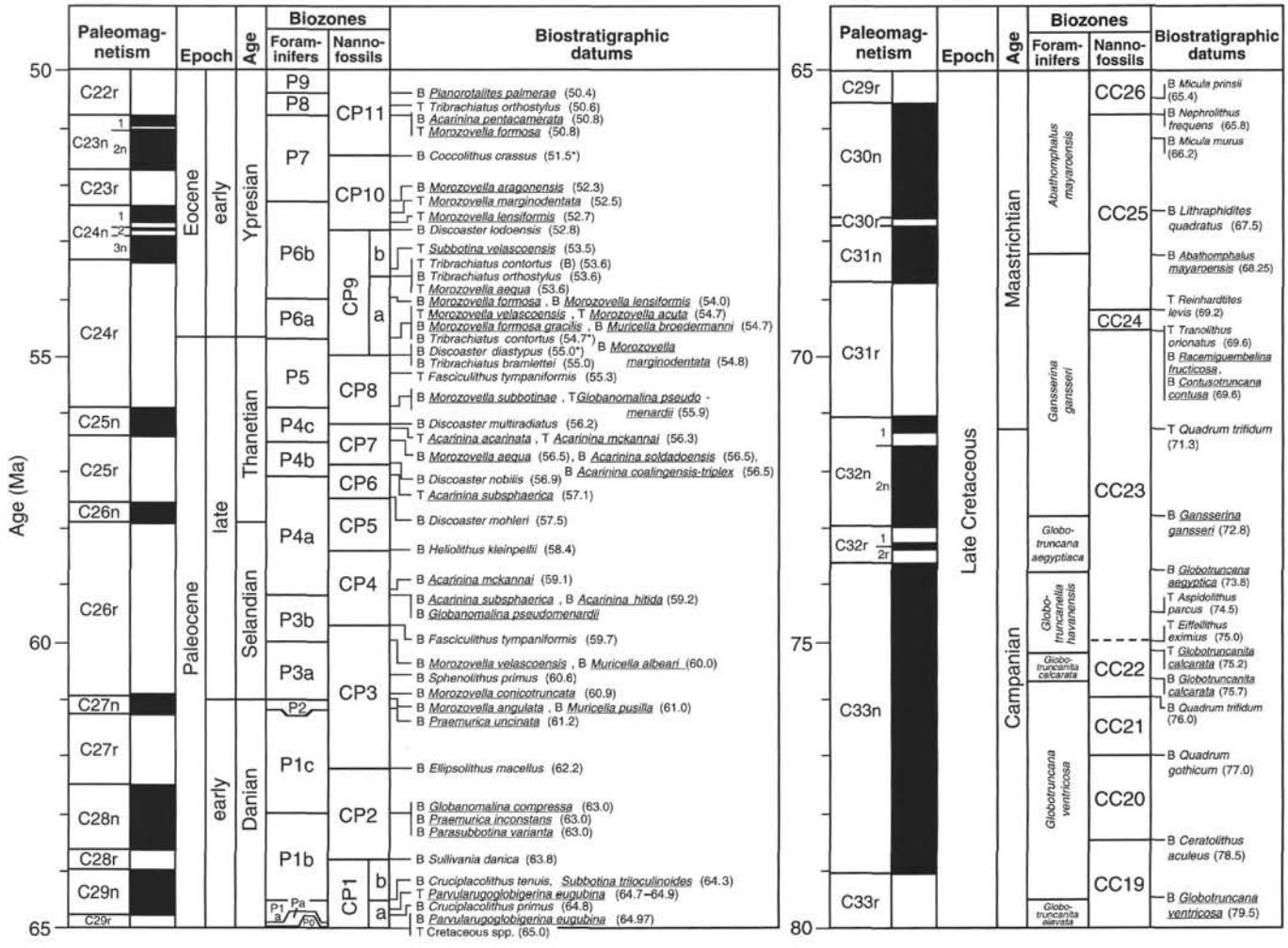

Figure 8 (continued).

Five levels of relative abundance were recorded as follows:

A = abundant (the taxonomic category comprises >10% of the total assemblage);
C = common (the taxonomic category comprises from 1% to 10% of the total assemblage);
F = few (the taxonomic category comprises from 0.1% to 1% of the total assemblage);
R = rare (the taxonomic category comprises <0.1% of the total assemblage); and
B = barren.

Planktonic Foraminifers

Zonation and Taxonomy

Taxonomic concepts for the Cenozoic planktonic foraminifers follow those of Kennett and Srinivasan (1983), Bolli and Saunders (1985), Toumarkine and Luterbacher (1985), Chaisson and Leckie (1993), Leckie et al. (1993), Chaisson and Pearson (in press), and Pearson and Chaisson (in press). The tropical Neogene planktonic foraminifer "N-zonation" scheme used here follows Blow (1969), as modified by Kennett and Srinivasan (1983) (Fig. 8). The major modifications from Blow (1969) are:

1. Zone N4 was not subdivided because doubt has been cast on the reliability of the FO of *Globoquadrina dehiscens* for correlation outside of the Pacific. Premoli Silva and Spezzaferri (1990) and Spezzaferri and Premoli Silva (1991) found *G. dehiscens* in P22 in the Indian Ocean and Gulf of Mexico, respectively.
2. Kennett and Srinivasan (1983) subdivided Blow's Zone N17 using the FO of *Pulleniatina primalis.* This partition was not employed because of the irregular stratigraphic occurrence of *Pulleniatina primalis* in Caribbean and Atlantic sediments (Bolli and Saunders, 1985).
3. The base of N20 is defined by the FO of *Globorotalia* (*Menardella*) *miocenica* at 3.6 Ma (Curry, Shackleton, Richter, et al., 1995), rather than by the FO of "*Globorotalia pseudopima*" (Blow, 1969). The LO of *Globorotalia* (*Hirsutella*) *margaritae* marks the base of Zone N20 in some earlier stratigraphic schemes (e.g., Berggren and van Couvering, 1974). Berggren et al. (1985b) give an age of 3.6 Ma for the LO of *Globorotalia* (*Hirsutella*) *margaritae* and the FO of *Globorotalia* (*Menardella*) *miocenica.* The latter event was used as a datum because *Gr.* (*M.*) *miocenica* is more abundant than *Gr.* (*H.*) *margaritae* in the tropical Atlantic.
4. As early as 1973, Bolli and Premoli Silva questioned the stability of the *Truncorotalia truncatulinoides* datum at 2.0 Ma. Much of the problem stems from the difficulty of separating *T. truncatulinoides* from its presumed ancestor, *Truncorotalia tosaensis* (Kennett and Srinivasan, 1983). The "*truncatulinoides*" morphotype can no longer be considered a good approximation for the Pliocene/Pleistocene boundary. The FO of *T. truncatulinoides* is not found below the FO of *T. tosaensis*

and, therefore, can still be used as a datum for the base of Zone N22.

5. Both Bolli and Premoli Silva (1973) and Blow (1979) recognized the FO of "*Globigerina*" *calida calida* as a zone boundary. Bolli and Premoli Silva (1973) cite an age of 0.14 Ma, but no basis for the age estimate is provided. Blow's Zone N23 was therefore not differentiated from his Zone N22.

Ongoing research on the taxonomy and biostratigraphy of Paleogene planktonic foraminifers has necessitated our adoption of the recently published Paleogene tropical–subtropical "P-zonation" of Berggren et al. (1995) (Fig. 8). This zonation is a substantial modification of the one evolved by Berggren (1969), Berggren et al. (1985b), and Berggren and Miller (1988). In particular, the numbering system for zones in the Paleocene to early Eocene interval differs in several places from that of Berggren and Miller (1988). The following modifications have been made by Berggren et al. (1995):

1. Zone Pα of Berggren and Miller (1988) has been modified and divided into Zones P0 and Pa. Zone P0 is the interval between the LO of *Globotruncana* spp. and the FO of *Parvularugoglobigerina eugubina* (after Smit, 1982). Zone Pa is the total range of *P. eugubina.*
2. Subzone P1a has been redefined as the interval between the LO of *Parvularugoglobigerina eugubina* and the FO of *Subbotina triloculinoides.* Subzone P1b has been redefined as the partial range of *Subbotina triloculinoides* below the FO of *Globanomalina compressa* sensu stricto. Subzone P1c has been redefined as the partial range of *Globanomalina compressa* sensu stricto below the FO of *Praemurica uncinata.*
3. Berggren et al. (1995) have divided Zone P3 into Subzones P3a and P3b by the FO of *Igorina albeari,* which is a carinate descendant of *I. pusilla* and regarded as synonymous with *I. laevigata.*
4. Zone P4 of Berggren and Miller (1988) is unchanged, but is divided into three subzones by using the LO of *Acarinina subsphaerica* and the FO of *A. soldadoensis.* Note that the latter biohorizon was used by Blow (1979) as the base of his Zone P5.
5. Zone P5 is defined by Berggren et al. (1995) as bounded at its base by the LO of *Globanomalina pseudomenardii* and at its top by the LO of *Morozovella velascoensis.*
6. Zone P6 is amended as the interval from the LO of *M. velascoensis* to the FO of *M. aragonensis.* The FO of *M. formosa* is used to divide the zone, so that Subzone P6a of Berggren et al. (1995) = Subzone P6b of Berggren and Miller (1988) = Zone P7 of Blow (1979), and Subzone P6b of Berggren et al. (1995) = Subzone P6c of Berggren and Miller (1988) = Subzone P8a of Blow (1979).

For the Paleocene interval, we followed the taxonomy of the *Atlas of Paleocene Planktonic Foraminifers* (Paleogene Working Group on Planktonic Foraminifers, in press).

Zones P7 through P22 of Berggren et al. (1995) are largely unchanged from Berggren and Miller (1988), but differ from the numerical coding of Blow (1979) (see discussions in Berggren and Miller, 1988).

The well-established zonal scheme of Caron (1985) was used for the Cretaceous. Except where otherwise noted, we followed the taxonomic concepts of Postuma (1971), Robaszynski and Caron (1979), Robaszynski et al. (1984), and Caron (1985) for Late Cretaceous trochospiral taxa and those of Nederbragt (1991) for Late Cretaceous serial taxa.

A list of planktonic foraminifer datums used in this study is presented in Table 3, which mainly follows Berggren et al. (1995, 1985b) with various modifications.

Methods

Sample preparation procedures varied according to the degree of lithification of the sample. Unlithified ooze was either washed directly in tap water or soaked briefly in a weak Calgon/hydrogen peroxide solution, then washed over a 63-μm mesh sieve. A 45-μm sieve was used through intervals in the upper Eocene and near the Cretaceous/Tertiary boundary to retain microtektites and tiny specimens of planktonic foraminifers. Semilithified ooze first was broken up partially by hand and then soaked in a weak Calgon solution before being washed and sieved. Chalk lumps were crushed and soaked in a hot Calgon solution before ultrasonic cleaning and a second soaking in weak Calgon solution before washing. Limestone samples were wrapped in a cotton towel, broken up with a ball peen hammer, soaked in a hot Calgon/hydrogen peroxide solution, and ultrasonicated for up to 20 min. All samples were dried at approximately 50°C on a hotplate.

The following abundance categories were estimated from a visual examination of the dried sample:

A = abundant (>30%),
C = common (15%–30%),
F = few (3%–15%),
R = rare (<3%), and
B = barren.

Preservation was estimated in the following categories:

G = good (>90% of the specimens unbroken; few signs of dissolution),
M = moderate (30%–90% of specimens broken or dissolved), and
P = poor (<30% of specimens intact).

Sedimentation Rates and Mass Accumulation Rates

To determine sedimentation rates, one must first generate an age-depth relationship. At a site with precisely determined paleomagnetic stratigraphy and with unambiguously identified chrons, accumulation rate uncertainties arise almost entirely from uncertainties in the ages of reversal boundaries.

Where biostratigraphic datums are used, the chief uncertainty arises from the fact that, with a limited amount of time for study, many datums are determined among widely separated samples. During many ODP legs, it has been necessary to reconstruct sedimentation rates using datums determined only in core catchers (i.e., within 9.5 m). The amount of uncertainty in each sedimentation rate estimate derived in this way is related to the thickness interval over which it is averaged, divided by the combined uncertainty in the top and bottom controls. At a sedimentation rate of 20 m/m.y., datums spaced at 9.5-m intervals would only allow breaking the accumulation rates into roughly 4-m.y. increments, if we aim for an uncertainty better than about ±20%.

The second source of uncertainty in sedimentation rates is the age of the datums, which of course increases as the uncertainty in the datum ages increases. Our aim is to use a prime set of datums, distributed less than 2 m.y. apart, and to determine these datums in all sites to within one section (1.5 m) or better.

Sedimentation rates (m/m.y.) may be estimated from age-vs.-depth plots either by drawing best-fit lines through all the biostratigraphic and paleomagnetic data over successive depth intervals, or by drawing straight-line segments. Inspection of the distribution of other datums about the lines suggests that it might be difficult to justify rigorously one approach vs. another, especially given the difficulty of evaluating the uncertainties in the accuracy of each datum. Plots of sedimentation rate vs. age are derived from the distribution of age-vs.-depth data. Age-vs.-depth plots, therefore, give more di-

rect evidence for or against rapid changes in sedimentation rate, which might otherwise be artificially exaggerated by using best-fit lines through discrete intervals of data. All sedimentation rates were calculated using midpoints in the observed depth uncertainty range. Note also that we only show uncertainties in depth in our sedimentation rate graphs. In reality, each datum event has an age uncertainty that may vary from a few thousand years to a few hundred thousand years.

Bulk sediment mass accumulation rates (MARs; g/cm^2/k.y.) are calculated from linear sedimentation segments and dry bulk density data (grams dry sediment per wet volume). Only those samples with both dry-bulk density and nearby carbonate data were used to calculate MARs. Carbonate MARs were calculated by multiplying bulk sediment MARs by percent carbonate; the noncarbonate MARs represent the difference between bulk and carbonate MARs. Ages were interpolated for all samples based on the linear sedimentation rate segments. Higher frequency variations in percentage of carbonate obviously imply that higher frequency variations in accumulation of either carbonate or noncarbonate are superimposed on relatively stable long-term accumulation rates. Variable preservation of the carbonate fraction may also play a role.

PALEOMAGNETISM

Laboratory Facilities and Procedures

The remanent magnetization of archive half sections was measured on a 2G Enterprises 760R magnetometer typically using a standard 10-cm reading interval before and after alternating-field (AF) demagnetization. The demagnetization treatment applied to these sections, usually one or two AF demagnetization steps, was selected based on the results of progressive AF demagnetization experiments conducted on pilot sections from the archive half and discrete samples from the working half. Peak AF demagnetizations on the archive half never exceeded 25 mT.

Magnetic susceptibility was measured for each whole-core section as part of the multisensor track (MST) analyses. The volume susceptibility values were recorded in 10^{-6} cgs units during Leg 165. Susceptibility values in SI units are 4π those in cgs units. Discrete sample remanence measurements were made with a new Molspin Minispin magnetometer, which replaced an older model Minispin magnetometer at the beginning of Leg 165. The spinner and cryogenic magnetometers were cross-calibrated and compared with a shipboard standard and with a standard measured previously at the University of Rhode Island laboratory.

The Schonstedt alternating field demagnetizer (GSD-1) and the Schonstedt thermal demagnetizer (TSD-1) permitted demagnetization to levels of 100 mT and 800°C, respectively. We avoided using peak fields above 50 mT on nearly all samples because of an anhysteretic remanent magnetization (ARM) imparted to the samples by the AF demagnetizer at high fields.

Core Orientation

All paleomagnetic measurements made during Leg 165 on the split-core sections and discrete samples follow the standard ODP core orientation scheme (Fig. 9). During drilling with the APC, core orientation was achieved with a Tensor orientation tool. Data from the Tensor tool were corrected for local magnetic variation before being used to compute remanence field directions. Oriented discrete samples were taken from the working half cores by (1) pressing a 6-cm^3 sample cube into soft sediment, (2) pressing a 2 × 2 cm stainless steel minicorer into the core and extruding the subcore into a 5-cm^3 sample cube, or (3) drilling a 2.5-cm diameter minicore. To minimize sediment deformation, either a thin stainless steel spatula or a saw was used to cut into more lithified sediment before insertion of the sample cubes.

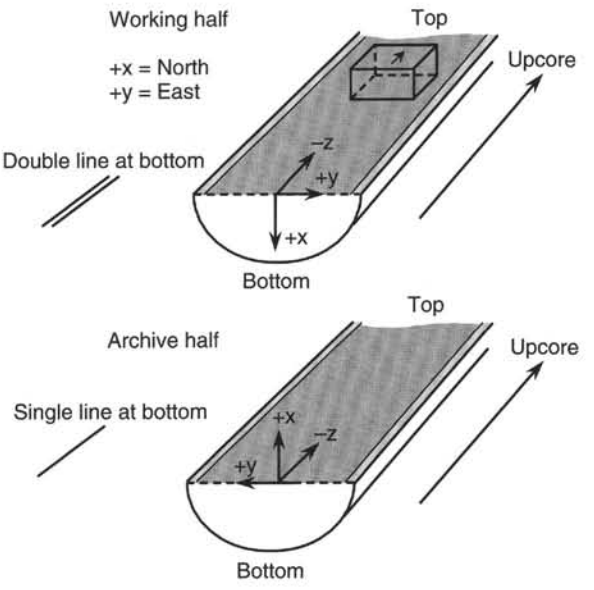

Figure 9. Paleomagnetic core orientation conventions for split-core sections and discrete samples.

Magnetic Polarity Reversal Time Scale

The magnetic polarity time scale for Leg 165 (Table 4) is a composite of five previous time scales: (1) Shackleton et al.'s (1990) astronomically tuned time scale for the interval from 0.0 to 2.6 Ma, (2) with the addition of the Cobb Mountain and Réunion event ages from Berggren et al. (1995); (3) Hilgen's (1991a, 1991b) astronomically tuned time scale for the interval from 2.6 to 5.23 Ma; (4) Shackleton et al.'s (1995, table 17) time scale (partially astronomically tuned) for the interval from 5.23 to 14.8 Ma; and, finally, (5) Cande and Kent's (1995) seafloor spreading-based time scale for ages older than 14.8 Ma. These five separate time scales are compatible and should not introduce artificial discontinuities in calculated sedimentation rates at the points where they have been joined.

Drilling-Induced Overprints

Overprints acquired during drilling and/or recovery of the core are common. They generally occur as an axial and a radial component. The axial component appears to dominate, as evidenced by the common steep inclinations that were measured during Leg 165 as well as on prior legs. Given the latitude of the sites in Leg 165, such steep inclinations are unexpected.

For whole cores, the vector sum of the radial overprint component should be zero or extremely small because the individual radial vectors cancel each other. This effect would further increase the likelihood of observing steep inclinations. Split-core sections rather than whole-core sections are measured in the magnetometer, however, which results in a vector sum for the radial component that is directed along a line perpendicular to the split-core surface (Fig. 10). For Leg 165, the natural remanent magnetization (NRM) is commonly directed downward at a steep angle (> +50°) and toward the north (declinations of ~0°). Given the orientation of the +X-axis for the archive half as measured by the magnetometer (Fig. 9), the northerly magnetization direction would indicate that the radial component is directed

Table 4. Ages used for the magnetic polarity time scale.

Boundary	Age (Ma)	Reference
	0.000	
C1n "Brunhes" (o)	0.780	SBP90
C1r.1n "Jaramillo" (t)	0.990	SBP90
C1r.1n "Jaramillo" (o)	1.070	SBP90
C1r.2r.1n "Cobb Mtn." (t)	1.201	BKSA95
C1r.2r.1n "Cobb Mtn." (o)	1.211	BKSA95
C2n "Olduvai" (t)	1.770	SBP90
C2n "Olduvai" (o)	1.950	SBP90
C2r.1n "Reunion" (t)	2.140	BKSA95
C2r.1n "Reunion" (o)	2.150	BKSA95
C2An.1n "Gauss" (t)	2.600	SBP90/H91
C2An.1r "Kaena" (t)	3.040	H91
C2An.1r "Kaena" (o)	3.110	H91
C2An.2r "Mammoth" (t)	3.220	H91
C2An.2r "Mammoth" (o)	3.330	H91
C2Ar "Gilbert" (t)	3.580	H91
C3n.1n "Cochiti" (t)	4.180	H91
C3n.1n "Cochiti" (o)	4.290	H91
C3n.2n "Nunivak" (t)	4.480	H91
C3n.2n "Nunivak" (o)	4.620	H91
C3n.3n "Sidufjall" (t)	4.800	H91
C3n.3n "Sidufjall" (o)	4.890	H91
C3n.4n "Thvera" (t)	4.980	H91
C3n.4n "Thvera" (o)	5.230	H91/SCHPS95
C3A.n1 (t)	5.875	SCHPS95
C3A.n1 (o)	6.122	SCHPS95
C3A.n2 (t)	6.256	SCHPS95
C3A.n2 (o)	6.555	SCHPS95
C3Bn (t)	6.919	SCHPS95
C3Bn (o)	7.072	SCHPS95
C3Br.1n (t)	7.135	SCHPS95
C3Br.1n (o)	7.170	SCHPS95
C3Br.2n (t)	7.341	SCHPS95
C3Br.2n (o)	7.375	SCHPS95
C4n.1n (t)	7.406	SCHPS95
C4n.1n (o)	7.533	SCHPS95
C4n.2n (t)	7.618	SCHPS95
C4n.2n (o)	8.027	SCHPS95
C4r.1n (t)	8.174	SCHPS95
C4r.1n (o)	8.205	SCHPS95
C4An (t)	8.631	SCHPS95
C4An (o)	8.945	SCHPS95
C4Ar.1n (t)	9.142	SCHPS95
C4Ar.1n (o)	9.218	SCHPS95
C4Ar.2n (t)	9.482	SCHPS95
C4Ar.2n (o)	9.543	SCHPS95
C5n.1n (t)	9.639	SCHPS95
C5n.1n (o)	9.775	SCHPS95
C5n.2n (t)	9.815	SCHPS95
C5n.2n (o)	10.839	SCHPS95
C5r.1n (t)	10.943	SCHPS95
C5r.1n (o)	10.991	SCHPS95
C5r.2n (t)	11.373	SCHPS95
C5r.2n (o)	11.428	SCHPS95
C5An.1n (t)	11.841	SCHPS95
C5An.1n (o)	11.988	SCHPS95
C5An.2n (t)	12.096	SCHPS95
C5An.2n (o)	12.320	SCHPS95
C5Ar.1n (t)	12.605	SCHPS95
C5Ar.1n (o)	12.637	SCHPS95
C5Ar.2n (t)	12.705	SCHPS95
C5Ar.2n (o)	12.752	SCHPS95
C5AAn (t)	12.929	SCHPS95
C5AAn (o)	13.083	SCHPS95
C5ABn (t)	13.252	SCHPS95
C5ABn (o)	13.466	SCHPS95
C5ACn (t)	13.666	SCHPS95
C5ACn (o)	14.053	SCHPS95
C5ADn (t)	14.159	SCHPS95
C5ADn (o)	14.607	SCHPS95
C5Bn.1n (t)	14.800	SCHPS95/CK95
C5Bn.1n (o)	14.888	CK95
C5Bn.2n (t)	15.034	CK95
C5Bn.2n (o)	15.155	CK95
C5Cn.1n (t)	16.014	CK95
C5Cn.1n (o)	16.293	CK95
C5Cn.2n (t)	16.327	CK95
C5Cn.2n (o)	16.488	CK95
C5Cn.3n (t)	16.556	CK95
C5Cn.3n (o)	16.726	CK95
C5Dn (t)	17.277	CK95
C5Dn (o)	17.615	CK95
C5En (t)	18.281	CK95
C5En (o)	18.781	CK95
C6n (t)	19.048	CK95
C6n (o)	20.131	CK95
C6An.1n (t)	20.518	CK95
C6An.1n (o)	20.725	CK95
C6An.2n (t)	20.996	CK95
C6An.2n (o)	21.320	CK95
C6AAn (t)	21.768	CK95
C6AAn (o)	21.859	CK95
C6AAr.1n (t)	22.151	CK95
C6AAr.1n (o)	22.248	CK95
C6AAr.2n (t)	22.459	CK95
C6AAr.2n (o)	22.493	CK95
C6Bn.1n (t)	22.588	CK95
C6Bn.1n (o)	22.750	CK95
C6Bn.2n (t)	22.804	CK95
C6Bn.2n (o)	23.069	CK95
C6Cn.1n (t)	23.353	CK95
C6Cn.1n (o)	23.535	CK95
C6Cn.2n (t)	23.677	CK95
C6Cn.2n (o)	23.800	CK95
C6Cn.3n (t)	23.999	CK95
C6Cn.3n (o)	24.118	CK95
C7n.1n (t)	24.730	CK95
C7n.1n (o)	24.781	CK95
C7n.2n (t)	24.835	CK95
C7n.2n (o)	25.183	CK95
C7An (t)	25.496	CK95
C7An (o)	25.648	CK95
C8n.1n (t)	25.823	CK95
C8n.1n (o)	25.951	CK95
C8n.2n (t)	25.992	CK95
C8n.2n (o)	26.554	CK95
C9n (t)	27.027	CK95
C9n (o)	27.972	CK95
C10n.1n (t)	28.283	CK95
C10n.1n (o)	28.512	CK95
C10n.2n (t)	28.578	CK95
C10n.2n (o)	28.745	CK95
C11n.1n (t)	29.401	CK95
C11n.1n (o)	29.662	CK95
C11n.2n (t)	29.765	CK95
C11n.2n (o)	30.098	CK95
C12n (t)	30.479	CK95
C12n (o)	30.939	CK95
C13n (t)	33.058	CK95
C13n (o)	33.545	CK95
C15n (t)	34.655	CK95
C15n (o)	34.940	CK95
C16n.1n (t)	35.343	CK95
C16n.1n (o)	35.526	CK95
C16n.2n (t)	35.685	CK95
C16n.2n (o)	36.341	CK95
C17n.1n (t)	36.618	CK95
C17n.1n (o)	37.473	CK95
C17n.2n (t)	37.604	CK95
C17n.2n (o)	37.848	CK95
C17n.3n (t)	37.920	CK95
C17n.3n (o)	38.113	CK95
C18n.1n (t)	38.426	CK95
C18n.1n (o)	39.552	CK95
C18n.2n (t)	39.631	CK95
C18n.2n (o)	40.130	CK95
C19n (t)	41.257	CK95
C19n (o)	41.521	CK95
C20n (t)	42.536	CK95
C20n (o)	43.789	CK95
C21n (t)	46.264	CK95
C21n (o)	47.906	CK95
C22n (t)	49.037	CK95
C22n (o)	49.714	CK95
C23n.1n (t)	50.778	CK95
C23n.1n (o)	50.946	CK95
C23n.2n (t)	51.047	CK95
C23n.2n (o)	51.743	CK95
C24n.1n (t)	52.364	CK95
C24n.1n (o)	52.663	CK95
C24n.2n (t)	52.757	CK95
C24n.2n (o)	52.801	CK95
C24n.3n (t)	52.903	CK95
C24n.3n (o)	53.347	CK95
C25n (t)	55.904	CK95
C25n (o)	56.391	CK95
C26n (t)	57.554	CK95
C26n (o)	57.911	CK95
C27n (t)	60.920	CK95
C27n (o)	61.276	CK95
C28n (t)	62.499	CK95
C28n (o)	63.634	CK95
C29n (t)	63.976	CK95
C29n (o)	64.745	CK95
C30n (t)	65.578	CK95
C30n (o)	67.610	CK95
C31n (t)	67.735	CK95
C31n (o)	68.737	CK95

Table 4 (continued).

Boundary	Age (Ma)	Reference
C32n.1n (t)	71.071	CK95
C32n.1n (o)	71.338	CK95
C32n.2n (t)	71.587	CK95
C32n.2n (o)	73.004	CK95
C32r.1n (t)	73.291	CK95
C32r.1n (o)	73.374	CK95
C33n (t)	73.619	CK95
C33n (o)	79.075	CK95
C34n (t)	83.000	CK95
C34n (o)	118.000	CK95

Notes: (t) = termination; (o) = onset. SBP90 = Shackleton et al. (1990); H91 = Hilgen (1991); CK95 = Cande and Kent (1995); BKSA95 = Berggren et al. (1995); SCHPS95 = Shackleton et al. (1995).

inward (toward the center of the core), if the northerly component has an overprint origin.

Because the cores are azimuthally unoriented, this bias for northward-trending declinations is unlikely to have any relationship to the ancient magnetization of the core (e.g., it is unlikely a Brunhes overprint). Ambient magnetic fields within the sensor region of the magnetometer could produce an induced magnetization that would have a common orientation relative to the split core. For cores with weak magnetization, a strongly magnetized sample holder could also be the source of constant directional biases.

ORGANIC GEOCHEMISTRY

The shipboard organic geochemistry program for Leg 165 included (1) real-time monitoring of volatile hydrocarbon gases; (2) measurement of the inorganic carbon concentration to determine the amount of carbonate in the sediments; (3) elemental analyses of total carbon, total nitrogen, and total sulfur; and (4) preliminary characterization of organic matter. All methods and instruments used during Leg 165 are described below. Additional details are available in Emeis and Kvenvolden (1986). These analyses were conducted as part of the routine shipboard safety requirements and to provide information for preliminary site summaries and shore-based organic geochemical research.

Hydrocarbon Gases: Sampling

During Leg 165, the compositions and concentrations of volatile hydrocarbons and other gases in the sediments were monitored at intervals of generally one per core. The headspace method was used throughout the cruise (Sites 998, 999, 1000, and 1001); gases released by the sediments after core recovery were analyzed by gas chromatography (GC) by means of the following technique. Immediately after retrieval on deck, a calibrated cork borer was used to obtain a measured volume of sediment from the end of one section of each core. The sediment sample, with a typical volume of approximately 5 cm^3, was placed in a 21.5-cm^3 glass serum vial that was sealed with a septum and metal crimp cap. When consolidated or lithified samples were encountered, chips of material were placed in the vial and sealed. Before gas analysis, the vial was heated in an oven at 60°C for 30 min. A 5-cm^3 volume of the headspace gas was extracted from each vial using a standard glass syringe. The collected gas was analyzed using gas chromatography.

The vacutainer method of gas analysis was used at Site 1002 when gas pockets or expansion voids were observed in cores as they arrived on deck. Vacutainers are pre-evacuated, septum-sealed glass tubes with a volume of 20 cm^3. For the purpose of obtaining a gas sample, a specially designed piercing tool is employed to penetrate the core liner. This tool, equipped with a valve and needle, is used to transfer gas from the core to the vacutainer.

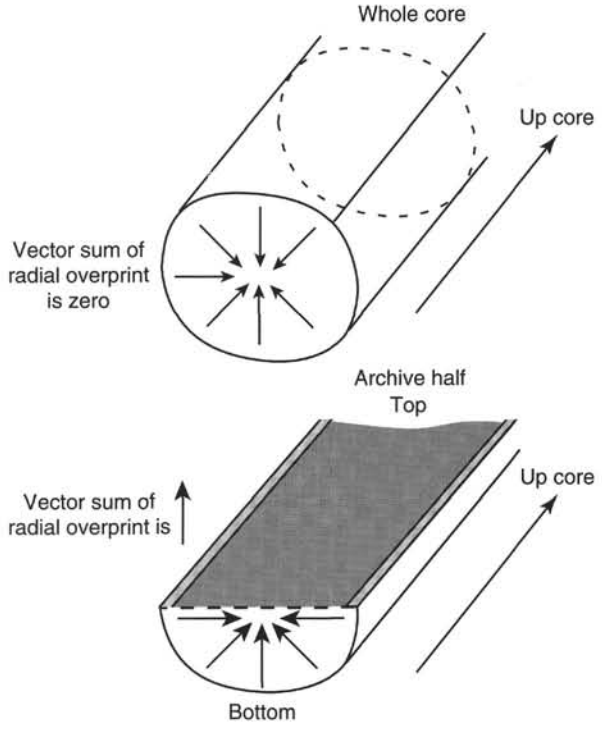

Figure 10. A radial overprint component, such as that indicated by the arrows, would sum to zero for the whole core but could be significant for the split core.

Hydrocarbon and Other Gases: Analysis

Samples of volatile hydrocarbons (i.e., headspace gases) were analyzed using the Natural Gas Analyzer (NGA), which routinely measures hydrocarbons through C_6. This system consists of a Hewlett-Packard 5890 II Plus gas chromatograph equipped with a 60 m × 0.32 mm DB-1 capillary column and a flame ionization detector (FID). Nonhydrocarbon gases (N_2, O_2, CO_2, and H_2S) were analyzed at the same time by means of a packed column and a thermal conductivity detector (TCD). For hydrocarbon analysis, the GC oven was heated to 40°C for 10 min and then ramped to 80°C at 4°C/min, yielding a total analysis time of 20 min. Helium was the carrier gas, and a Hewlett Packard Chemstation was used for data acquisition and processing. Chromatographic response was calibrated against preanalyzed standards; gas contents are reported in parts per million (ppmv). The second shipboard Hewlett Packard 5890 II Plus gas chromatograph, which is normally dedicated to rapid analysis of methane/ethane ratios, was not available during the first half of Leg 165. Once available, the results from this instrument compared favorably with those of the NGA. Consequently, the NGA was used for the remainder of Leg 165.

Inorganic Carbon

Carbonate carbon concentrations were determined using a Coulometrics 5011 carbon-dioxide coulometer. Routinely, one carbonate determination was performed for each 1.5-m section of core. A sample of approximately 10 mg of freeze-dried, ground sediment was reacted with 2N HCl. The liberated CO_2 was back-titrated to a colorimetric endpoint. Percentage of carbonate is calculated from the inorganic carbon (IC) content with the assumption that all inorganic carbon is present as calcium carbonate:

$$CaCO_3 = IC \times 8.33.$$

Elemental Analyses

Total carbon, nitrogen, and sulfur were determined using a Carlo Erba 1500 CNS Analyzer. Sediments were analyzed at a frequency of generally one sample per every one to two cores. Approximately 5 mg of freeze-dried, ground sediment were combusted at 1000°C in a stream of oxygen. Using He as a carrier gas, the oxygen was removed and the combustion products were reduced. The reduced gases were separated by gas chromatography and quantified with a TCD. Contents of total organic carbon (TOC) were calculated as the difference between total carbon (TC) and inorganic carbon (IC):

$$TOC = TC - IC.$$

Organic Matter Characterization and Determination of Maturity

The type of organic matter in a selected group of samples (~100 mg) was also characterized by pyrolysis, using a Delsi Nermag Rock-Eval II system. This method is based on a whole-rock pyrolysis technique designed to identify the type and maturity of organic matter and to detect the petroleum potential of the sediments (Tissot and Welte, 1984; Espitalié et al., 1986). The Rock-Eval system includes a temperature program that first releases volatile hydrocarbons (S_1) at 300°C for 3 min. Hydrocarbons are then released by means of thermal cracking of kerogen (S_2) as the temperature is increased from 300° to 550°C at 25°C/min. S_1 and S_2 hydrocarbons are measured by an FID and reported in milligrams per gram of sediment. The temperature at which the kerogen yields the maximum amount of hydrocarbon during the S_2 program provides T_{max}, a parameter used to assess the maturity of the organic matter. Between 300° and 390°C of the stepped pyrolysis, CO_2 released from the thermal degradation of organic matter (S_3) is trapped and measured by a TCD in milligrams per gram of sediment. Rock-Eval II parameters help in characterizing organic matter by allowing the following indexes to be calculated: hydrogen index (HI; $100 \times S_2/TOC$), oxygen index (OI; $100 \times S_3/TOC$), S_2/S_3 ratio, and productivity index (PI; $S_1/(S_1 + S_2)$). Interpretation of Rock-Eval data is considered to be compromised for samples containing less than 0.5% TOC (Peters, 1986).

INORGANIC GEOCHEMISTRY

Interstitial Waters

Shipboard interstitial water analyses were performed on 5-cm-long, whole-round sections cut immediately after core retrieval on deck. Because each site was single recovery (with the exception of Site 1002 in the Cariaco Basin), the size of the IW sample was not increased to 15-cm whole rounds deeper in the hole for core preservational purposes. Where possible, samples were taken from the bottom of Section 3 of the first core and every third core thereafter (i.e., Cores 1H, 3H, 6H, etc.).

Interstitial waters were collected using the trace metal noncontaminating titanium squeezer, which is modified from the standard ODP stainless steel squeezer of Manheim and Sayles (1974). After extrusion from the core liner in the chemistry laboratory, the surface of each whole round was carefully scraped with a spatula to remove potential contamination. This scraped excess material was saved and archived for future research (e.g., paleontology). After loading the squeezer, pore waters were extruded by applying pressures up to 40,000 lb (approximately 4150 psi) using a hydraulic press. Interstitial water samples were collected into plastic syringes and subsequently filtered through 0.45-µm Gelman polysulfone disposable filters and stored in plastic vials before being analyzed. Aliquots for post-cruise, shore-based analyses by the shipboard scientists were retained in heat-sealed, acid-washed plastic tubes and glass vials.

Interstitial water samples were routinely analyzed for salinity, as total dissolved solids (g/kg), with a Goldberg optical hand-held refractometer (Reichart); for pH and alkalinity by Gran titration with a Brinkmann pH electrode and a Metrohm autotitrator; and for silica, phosphate, and ammonium by spectrophotometric methods with a Milton Roy Spectronic 301 spectrophotometer (Gieskes et al., 1991). International Association of Physical Sciences Organizations (IAPSO) standard seawater was used for calibrating most techniques, and for determining 1σ standard deviations. These standard deviations were alkalinity = <1.5%, chloride = 0.4%, calcium = <1%, magnesium = 0.5%, and silica and ammonia = ~5%.

In addition, potassium, magnesium, calcium, and sulfate were analyzed by ion chromatography using a Dionex DX-100 (Cline, 1969). The 1σ standard deviations were potassium = <3%, magnesium and calcium = <3%, sulfate = <4%, and sodium = <5%.

Lithium, potassium, manganese, strontium, and iron concentrations were quantified using flame atomic absorption spectrometry (Varian SpectrAA-20). Iron was determined on undiluted 5-mL aliquots acidified with 100 µL of concentrated HCl; manganese was determined on 1/5 diluted samples, as well as lithium and strontium on 1/10 diluted samples (and higher as needed), using an air-acetylene (Fe, Li, K, Mn) and nitrous oxide acetylene flame (Sr). Standards for all flame AES techniques were matched in matrix composition to the samples. A more detailed description of all methods and standards used can be found in ODP Technical Note 15 (Gieskes et al., 1991).

Sediment, Volcanic Ash, and Basalt Chemistry

In addition, during Leg 165 we undertook an ambitious major and trace element sediment chemistry program designed to provide rapid results to aid in shipboard sampling and identification of key lithologic sections. As described below, we routinely analyzed a 10-cm^3 sediment sample from each core at each site. This large-volume sample was required for X-ray fluorescence (XRF) analysis (see below). Details of the sampling resolution are described in the individual site chapters (this volume). Because of the high frequency of ash layers, 15-cm^3 samples from select ash layers were also analyzed. Representative samples of basalt from the igneous basement at Site 1001 were also analyzed.

Sediment samples were acquired from the sampling table, freeze-dried in the chemistry laboratory, and powdered and homogenized by hand with an agate mortar and pestle. Approximately 6 g of unfired sediment sample powder was mixed with 40 to 50 drops of Chemplex liquid polymer binder and pressed into an aluminum Spex-cap at 5 to 7 tons of pressure using a hydraulic press.

Ash samples were ground on a diamond-grit grinding wheel to remove saw marks and any outside surfaces exposed to the coring bit. Samples were then sonicated in distilled water and dried in a 110°C oven for over 5 hr. Cleaned rock chips were reduced to a fine gravel (≤5 mm pieces) by crushing the chips between two pieces of Delrin plastic in a hydraulic press, and ground to a powder (≤200 mesh) in a WC shatterbox. Powders to be analyzed for major elements were ignited for 8 to 10 hr at 900°C to determine loss on ignition and to oxidize all iron to the trivalent state. Duplicate glass disks of each sample were prepared by fusing 0.500 g of ignited sample powder with 6.00 g of a lanthanum-bearing lithium borate flux in a modified Claisse fluxer. Ash samples for trace element analysis were prepared identically to the sediments (described above).

For sediment, basalt, and ash samples, major and trace element abundances were determined using an automated ARL 8420 wavelength-dispersive spectrograph, equipped with an end-window, Rh-target X-ray tube, under measuring conditions outlined in Tables 5 and 6. Sediment and ash trace element analyses (Nb, Zr, Y, Sr, Rb, Zn, Cu, Ni, Cr, V, and Ba) were performed on the pressed pellets and corrected for nonlinear backgrounds, spectral interferences, and matrix absorption effects using the ARL software package and a range of geologic standards. Because ignited powders were used for the ash

Table 5. XRF operating conditions for ash major elements, and both ash and sediment trace elements.

Oxide/ element	Line	Crystal	Detector	Collimator	Peak angle (°2θ)	Background offset (°2θ)	Total count time	
							Peak (s)	Background (s)
SiO_2	Kα	PET(002)	FPC	Medium	109.21	0	40	0
TiO_2	Kα	LiF(200)	FPC	Fine	86.11	0	40	0
Al_2O_3	Kα	PET(002)	FPC	Medium	145.18	0	100	0
Fe_2O_3*	Kα	LiF(200)	FPC	Fine	57.47	0	40	0
MnO	Kα	LiF(200)	FPC	Fine	62.93	0	100	0
MgO	Kα	TLAP(1010)	FPC	Medium	45.17	±0.80	150	150
CaO	Kα	LiF(200)	FPC	Medium	113.12	0	40	0
Na_2O	Kα	TLAP(1010)	FPC	Medium	55.1	−1.20	150	150
K_2O	Kα	LiF(200)	FPC	Medium	136.69	0	100	0
P_2O_5	Kα	Ge(111)	FPC	Medium	141.09	0	100	0
Rh	Kα-Compton	LiF(200)	Scint	Fine	18.60	0	60	0
Nb	Kα	LiF(200)	Scint	Fine	21.40	−0.35	200	200
Zr	Kα	LiF(200)	Scint	Fine	22.55	−0.35	100	100
Y	Kα	LiF(200)	Scint	Fine	23.8	−0.40	100	100
Sr	Kα	LiF(200)	Scint	Fine	25.15	−0.40	100	100
Rb	Kα	LiF(200)	Scint	Fine	26.62	−0.60	100	100
Zn	Kα	LiF(200)	Scint	Medium	41.81	−0.40	100	100
Cu	Kα	LiF(200)	Scint	Fine	45.03	−0.40	100	100
Ni	Kα	LiF(200)	Scint	Medium	48.67	−0.60	100	100
Fe	Kα	LiF(220)	FPC	Fine	85.65	0	100	0
Cr	Kα	LiF(200)	FPC	Fine	69.35	−0.50	100	100
Ti	Kα	LiF(200)	FPC	Fine	86.18	0	40	0
V	Kα	LiF(220)	FPC	Fine	123.06	−0.50	100	100
Ce	Lα	LiF(220)	FPC	Medium	128.13	1.50	100	100
Ba	Lβ	LiF(220)	FPC	Medium	128.78	1.50	100	100

Notes: * = total Fe as Fe_2O_3. FPC = flow proportional counter using P10 gas. Scint = NaI scintillation counter. Trace elements analyzed under vacuum using generator settings of 50 kV and 50 mA. Major elements analyzed under vacuum using generator settings of 30 kV and 80 mA. The intensities for Rh, Fe, and Ti were used for trace element matrix corrections only. No associated concentrations were determined.

Table 6. XRF operating conditions for sediment major elements.

Oxide/ element	Spectral line	Analyzing crystal	Detector	Collimator	Peak angle (°2θ)	Background offset (°2θ)	Total count time	
							Peak (s)	Background (s)
Rh	Rh-Kα Compton	LiF(200)	Scint	Fine	18.565	0	60	0
Fe_2O_3*	Fe-Kα	LiF(200)	FPC	Fine	57.500	0.500	100	100
MnO	Mn-Kα	LiF(200)	FPC	Medium	62.980	0.700	100	100
TiO_2	Ti-Kα	LiF(200)	FPC	Medium	86.250	−1.000	100	100
CaO	Ca-Kβ	LiF(200)	FPC	Fine	100.220	0.600	20	20
P_2O_5	P-Kα	Ge(111)	FPC	Medium	141.030	−1.000	100	100

Notes: Same as in Table 5, except generator settings are 50 kV and 50 mA.

major element analyses, all ash major element analyses are reported on an anhydrous, CO_2-free basis, with total iron as Fe_2O_3 (Fe_2O_3*). Totals may tend to be slightly high as a result of the partial volatilization of sulfur during ignition. The major element calibration was determined by simple linear regression on a wide range of geologic standards. No matrix corrections were used because of the large flux to sample dilution ratio (12:1).

For the sediment, a smaller suite of major elements (Fe, Mn, Ti, P, and Ca) were measured separately on the same pressed pellet as was used for the trace element analysis. X-ray intensities were corrected for nonlinear backgrounds and spectral interferences after Norrish and Chappell (1977). Matrix absorption effects were corrected by using a modified Compton scattering method (Reynolds, 1963, 1967; Walker, 1973) to account for the overall major element content and the absorption edges of Fe, Ti, and Ca (Table 6). The absorption edge for K was assumed to be negligible and therefore was not accounted for.

For the sediment analysis, both precision and accuracy were assessed by multiple analysis of Standard Reference Material 1C, an argillaceous limestone from the National Institute of Standards and Technology (NIST) (Washington, DC, U.S.A.). For the ash analysis, references NIST-278 (rhyolite) and USGS G-2 (granite) were used. Precision values are given in Table 7.

Handling of K/T Boundary Sequence

Routine precautions for minimizing precious metal contamination of all cores were observed by the entire shipboard party within the core laboratory. This largely consisted of the removal of all jewelry before entering laboratories and handling cores. Cores were washed with "potable water" after splitting. In addition, special precautions were taken while handling core 3 m on either side of the K/T boundary. This section was designated as a critical interval. Because we recognize the many possibilities for contamination during coring and unavoidable shipboard handling, we made every effort to minimize contamination. The blade of the shipboard saw was cleaned rigorously with hydrogen peroxide and NANOpure water before cutting of the critical intervals. Once in the core laboratory, clean gloves were worn during any work involving these intervals. Sample manipulation was conducted using ceramic, PTFE, HDPE and glass implements that had been previously cleaned for several days. The cleaning sequence involved (1) soaking the implements for 8 hr in 30% trace metal grade hydrogen peroxide, which was found to be particularly effective at removing trace organo-metallic contaminants that often contain elevated levels of W and Zn; (2) rinsing the implements with 18 megaohm NANOpure water; (3) soaking the implements again for 8 hr in aqua regia made up from double quartz distilled, sub-

Table 7. Precision determinations for major and trace element analysis of sedimentary and igneous rock reference samples.

	Average	SD	Average	SD
Trace elements (N = 28)				
	NBS-1C (argillaceous limestone)		NBS-278 (rhyolite)	
Nb	0.7	0.4	17.8	0.4
Zr	28.0	1.2	308	2
Y	2.38	0.87	43	1.4
Sr	244	1.3	57	0.5
Rb	11	0.6	129	1.2
Zn	34	0.9	36	0.8
Cu	16	0.8	5.9	0.4
Ni	12	1.0	4.3	0.7
Cr	14	0.7		
V	8.6	1.8	5.4	1.8
Ba	138	6.2	847	12
Ash major elements (N = 20)				
	G-2 (granite)			
SiO_2	69.7	0.4		
TiO_2	0.49	0.01		
Al_2O_3	15.60	0.13		
Fe_2O_3	2.84	0.02		
MnO	0.04	0.00		
MgO	0.94	0.02		
CaO	1.92	0.01		
Na_2O	4.15	0.06		
K_2O	5.22	0.02		
P_2O_5	0.13	0.00		
Sediment major elements (N = 8)				
CaO	51.8	0.4		
Fe_2O_3	0.62	0.0027		
MnO	0.03	0.0003		
P_2O_5	0.04	0.0005		
TiO_2	0.09	0.0004		

boiling concentrated nitric acid (Seastar, acid batch 7697-37-2; water batch 7732-18-5) and Fisher trace metal grade concentrated hydrochloric acid (acid batch 7647-01-0, water batch 7732-18-5); and (4) finally rinsing the implements with NANOpure water. Cleaned teflon beakers were used throughout this process. Small sample fragments for trace metal analysis were placed in glass vials cleaned using the above procedure.

One should note that the K/T boundary transition at Holes 999B and 1001A was recovered from the "core catcher" and initially placed on an aluminum tray, which may have contained small residues of other samples, before it reached the core lab. Loose samples lying on this tray were collected and designated as not suitable for trace metal work. In addition, the potentially contaminated nature of exterior fragments from those samples should be recognized.

These intervals were transferred to new core liners that had been cleaned in 30% trace metal grade hydrogen peroxide and 10% nitric acid, and then rinsed with NANOpure water. Of particular significance is the presence of a globule of "pipe dope" in the core-catcher lining of the section recovered from Hole 1001A. This material contains extremely high levels of Zn (>20 wt%), and its potential for severe metal contamination should be recognized here and elsewhere because of its sporadic appearance in other core liners. None of this material was observed in contact with any rock fragments. Shore-based analyses will further evaluate its potential for precious metal contamination. Intimate contact with plastic films was generally avoided, although the interval either side of the K/T boundary at Hole 999B was initially covered in Saran wrap before being color-scanned. This batch of Saran wrap had been previously characterized for trace metals by ODP chemists and found to contain sub-ppm levels.

IGNEOUS PETROLOGY AND VOLCANOLOGY

Core Curation and Shipboard Sampling

To preserve important features and structures, core sections containing igneous rocks were examined before being split. During core handling and splitting, core orientation was preserved by marking the base of individual pieces with a red chinagraph pencil. Each piece was numbered sequentially from the top of each core section and was labeled at the top surface. Pieces that could be fitted together were assigned the same number and were lettered consecutively (e.g., 1A, 1B, and 1C). Plastic spacers were placed between pieces having different numbers. The presence of a spacer may therefore represent a substantial interval of no recovery. After the vertical core orientation was noted, the pieces were split with a diamond-impregnated saw into archive and working halves, with care taken to ensure division of key features.

Nondestructive physical-properties measurements, such as magnetic susceptibility and natural gamma-ray emission, were taken on the core before it was split. After the core was split, the working half was sampled for shipboard physical properties, magnetic studies, XRF, XRD, and thin-section studies. Samples were taken from most of the lithologic units for thin-section studies and XRF major- and trace-element analysis. The archive half was described on the visual core description form and was photographed before storage.

Visual Core Descriptions

Visual core description forms were used when documenting the igneous rock cores (see "Lithostratigraphy" section, this chapter). The left column on the form is a graphic representation of the archive half. A horizontal line across the entire width of the column denotes a plastic spacer. Oriented pieces are indicated on the form by an upward-pointing arrow to the right of the piece. Shipboard samples and studies are indicated in the column headed "Shipboard Studies" with the following notation: D = XRD analysis, F = XRF analysis (in igneous basement, samples are labeled "XRF"), T = petrographic thin section (in igneous basement, thin-section samples are labeled "TSB"), P = physical-properties analysis, and M = paleomagnetic analysis. The core was divided into consecutively numbered lithologic units (mostly representing single lava flows) on the basis of changes in color, structure, grain size, and mineral occurrence and abundance.

The visual core descriptions were entered into the computer database HARVI. This database is divided into separate compartments

for fine- and coarse-grained rocks. All the volcanic rocks were entered into the fine-grained compartment. Each record is checked by the database program for consistency and completeness and is subsequently printed in a format that can be directly merged with the visual core description sheet to form a complete core section description. Separate HARVI records were made for each core section; and, if more than one lithologic unit was present in a section, separate records were made for each unit. Each HARVI record comprises the following information:

1. The leg, site, hole, core number and core type, and section number.
2. The unit number (consecutively downhole), the rock name (see below), and the number of pieces.
3. Contact relationships with neighboring lithologic units.
4. Phenocrysts: number of mineral phases visible with a hand lens or under a binocular microscope and their distribution within the unit; for each phase, its abundance (vol%), size range (mm), shape, degree of alteration, and further comments if appropriate.
5. Groundmass texture and grain size: glassy, aphanitic, fine-grained (<1 mm), medium-grained (1–5 mm), or coarse-grained (>5 mm), including any notations about grain-size changes within units.
6. Vesicles: abundance, distribution, size, shape, and mineral linings and fillings.
7. Color name and code (for the dry rock), according to Munsell Color Charts.
8. The rock structure: whether the unit is massive, flow-banded, flow-brecciated, scoriaceous, pillowed, hyaloclastic, or tuffaceous.
9. Alteration: alteration was graded as fresh (<5%), slight (5%–10%), moderate (10%–40%), strong (40%–90%), and complete (90%–100%), including any notations about changes in alteration through a section or a unit.
10. The presence of veins and fractures, including their abundance, width, mineral linings and fillings, and their orientations, where possible.
11. Additional comments, including notes on the variability of the unit.

The rocks were described as aphyric when no phenocrysts were visible with a hand lens or under a binocular microscope. The name "aphyric olivine basalt" was applied when olivine or its alteration products was considered to be present in the groundmass, whereas "aphyric basalt" was applied when little or no olivine was seen in the groundmass. Porphyritic rocks were named by phenocryst type, using mineral names in order of decreasing abundance. "Picrite" was defined as a rock having at least 15% olivine phenocrysts. The rock names were assigned initially on the basis of hand-specimen observation and were later checked with the thin sections, especially concerning the occurrence of olivine in the groundmass.

Thin-Section Descriptions

The thin sections of most of the lithologic units were examined to complement and refine the hand-specimen observations. The percentages of various components present in the thin sections either were estimated visually or were determined by counting 500 points, using an automatically advancing stage with an attached counter. The percentages and textural description of individual phases were reported in the database HRTHIN. All textural terms used were defined in MacKenzie et al. (1982). The terminology used for thin-section descriptions was also used for the visual core descriptions. For some porphyritic basalts, the thin-section and visual core descriptions differ slightly, primarily because small plagioclase laths in a rock with seriate texture are only visible in thin section. Thus, a rock visually described as olivine-plagioclase-phyric may be plagioclase-olivine-phyric, according to the thin-section description. This discrepancy has been accepted and retained to maintain consistency of the visual records because not all units were examined in thin section. Thin-section descriptions of igneous rock are given in Section 5 (this volume) and are also available in the HRTHIN database.

Rock Classification

In general, igneous rocks recovered during drilling were classified based on visual and thin-section examination. When samples were analyzed by XRF, however, the major element abundances were used to assign a rock name. For this purpose, we have used the compositional classification of Le Bas et al. (1986), which is based on a plot of total alkalis vs. silica content.

XRF Analysis

Samples representative of most of the lithologic units were selected for shipboard XRF analysis. Large pieces were reduced to a diameter of less than 1 cm by crushing between two disks of Delrin plastic in a hydraulic press. The sample was then ground for approximately 5 min in a Spex 8510 shatterbox with a tungsten carbide barrel.

A fully automated wavelength-dispersive ARL8420 XRF system equipped with a 3-kW generator and a Rh-anode X-ray tube was used to determine the major- and trace-element abundances in the samples. Analytical conditions used are given in Table 5. The spectrometer was calibrated using a suite of well-analyzed reference standards (AGV-1, AII-92, BE-N, BHVO-1, BIR-1, BR, DR-N, G-2, GH, JB2, JB#, JGB1, K1919, RGM-1, UB-N). The values recommended by Govindaraju (1989) were used for all elements, except for Zr and Nb. A subset of the standards, with concentrations recommended by Jochum et al. (1990), was used for these two elements. Precision estimates, based on replicate shipboard analyses of the USGS reference standard BIR-1, are given for major and trace elements in Table 7.

Major-element analyses were performed on fused lithium borate glass disk doped with lanthanum oxide as a heavy absorber (Norrish and Hutton, 1969). These disks were prepared from 500 mg of rock powder that had been ignited for 2 hr at about 1100°C, mixed with 6.000 g of dry flux that consisted of 80% lithium tetraborate and 20% lanthanum oxide. This mixture was then fused in air at 1150°C in a Pt-Au crucible for about 4 min, with constant agitation to ensure thorough mixing, and then poured into a Pt-Au mold. The 12:1 flux:sample ratio and the use of the heavy absorber make matrix effects insignificant over the normal range of igneous rock compositions. Hence, the relationship between X-ray intensity and element concentration is linear.

Trace elements were determined on pressed-powder pellets. These were made by mixing 7 g of rock powder with 30 drops of a solution of Chemplex polymer in methylene chloride (100 mg/cm^3) and then pressing the mixture into an aluminum cap under a load of 8 tons. A pellet made with 5 g of basalt powder should be infinitely thick with respect to X-rays at the shortest wavelengths used in the analysis. X-ray intensities were corrected for line-overlap and interelement adsorption effects. The latter corrections were based on the relationship between mass absorption coefficient and the intensity of the RhKα Compton scatter line (Reynolds, 1963, 1967; Walker, 1973).

PHYSICAL PROPERTIES

Introduction

Physical properties were measured on whole-round cores and the undisturbed parts of split cores. The multisensor track (MST) was used for nondestructive, whole-round core measurements of wet-bulk density, compressional-wave velocity, magnetic susceptibility, and natural gamma radiation. Needle-probe thermal conductivity measurements were also conducted on whole-round cores. Un-

drained shear strength, compressional-wave velocity and resistivity were measured on split sections. Portions of split cores that were not grossly disturbed by drilling were used to obtain specimens for index properties measurements (wet-bulk density, grain density, dry-bulk density, water content, and porosity). Three to seven discrete samples per core were selected based on the MST results.

Multisensor Track

The MST includes four physical properties sensors: magnetic susceptibility meter (MSM), gamma-ray attenuation porosity evaluator (GRAPE), *P*-wave logger (PWL), and natural gamma radiation detector (NGR). After the cores had thermally equilibrated (4 hr), individual, unsplit core sections were placed on the MST, which automatically moves the section through the four sensors on a fiberglass track.

MST data are sampled at discrete intervals, with the sampling rate chosen to optimize the resolution of the data and the time necessary to run each core section through the device. Magnetic susceptibility, GRAPE, and *P*-wave velocities were collected at 1- to 5-cm spacings, and NGR was sampled at 10- or 30-cm intervals. For part of Leg 165, the *P*-wave velocities were not measured because the PWL requires a completely filled core liner.

GRAPE measurements of wet-bulk density were made by comparing the gamma-ray attenuation of the sediments with the degree of attenuation through an aluminum standard (Boyce, 1976). The GRAPE device was calibrated at least every 24 hr. For Site 998, only the raw GRAPE data were collected, whereas for the remaining sites the raw data as well as the data corrected for the low neutron content of water were recorded (Boyce, 1976; Shipboard Scientific Party, 1994).

The high-resolution *P*-wave logger (PWL) continuously measured *P*-wave velocity orthogonal to the long-axis of whole-round core sections. PWL transmits 500-kHz compressional-wave pulses through the core at a rate of 1 kHz. The transmitting and receiving transducers were aligned perpendicular to the core axis while a pair of displacement transducers monitored the separation between the compressional wave transducers. Variations in the outside diameter of the liner do not degrade the accuracy of the velocities, but sediment must completely fill the liner for the PWL to provide accurate measurements. The PWL requires two types of calibrations, which were performed at the beginning of the leg: (1) the displacement transducer was calibrated using a standard core liner and a block standard; and (2) a one-point velocity calibration was done with the water standard.

Magnetic susceptibility was measured on all sections using the 1.0 range on the Bartington Model MS2 meter with an 8-cm diameter loop.

Natural gamma radiation analysis, which is a function of the random and discrete decay of radioactive atoms, was made with scintillation detectors according to the procedures outlined by Hoppie et al. (1994).

Thermal Conductivity

Thermal conductivity data were collected using the full-space, needle-probe method of Von Herzen and Maxwell (1959). Cores were first passively equilibrated to room temperature (nominally 17°C) for at least 4 hr. The needle probes were then inserted into the core through holes drilled in the liner. Care was taken to avoid insertion of the needle probes into visible voids or into liquid parts of the core. Four thermal conductivity needles were used simultaneously whenever possible. On each run, three needles measured thermal conductivity in the cores, while one needle was placed in a standard of black rubber, red rubber, or macor. Each of the four available needles was systematically rotated between standards during sequential runs.

Collection of thermal conductivity data was controlled by a preprogrammed microprocessor, the Thermcon-85. Before data collection, a drift survey measured temperature changes for a minimum of 120 s. Thermal conductivity data collection proceeded only when drift no longer exceeded 0.04°C/min for any of the needle probes. During the data collection phase, the microprocessor applied constant heat to each needle for 6 min. The reference voltage, the resistance measured by each of the probes, and the current were sequentially logged by the Thermcon unit.

To determine thermal conductivity, the measured resistances are first converted to temperatures using calibration constants and drift corrections for each needle. Apparent sediment thermal conductivity adjacent to a given needle probe is approximately proportional to the ratio of temperature and the natural logarithm of time, once a linear correction for drift has been included (Von Herzen and Maxwell, 1959). Most thermal conductivity determinations were made using data collected between 60 and 240 s from the beginning of the heating interval. For each needle, the data were fit using a least-squares regression procedure, which yields both the thermal conductivity and the rate of temperature change. Errors are typically between 5% and 10%. No corrections for temperature or pressure conditions were made as part of the thermal conductivity collection procedure (Ratcliffe, 1960).

P-wave Measurements on Split-Core Sections

P-wave velocities were measured directly on the core at discrete locations with the Dalhousie University/Bedford Institute of Oceanography digital sonic velocimeter (DSV) (Mayer et al., 1987; Courtney and Mayer, 1993). The T1 transducer pair has a fixed separation of 7.0 cm and is inserted along the axis of the core in soft sediments to measure velocity orthogonal to bedding. The T2 transducer (separation of 3.5 cm) measures velocity roughly parallel to bedding and is inserted perpendicular to the core's axis.

The velocity calculation is based on the traveltime of an impulsive acoustic signal between the piezoelectric transducers inserted in the split sediment cores. The transmitted signal is a 0.1 µs square wave with a period of 0.2 ms. The return signal is stored by the computer, and the first arrivals are hand picked. The DSV software then automatically calculates sediment velocity.

When the material became too consolidated to insert the DSV transducers, measurements were made through the core-barrel liner with the Hamilton Frame system. The velocity estimate is based on the traveltime between two contact transducers (T3 pair). One is placed on the cut surface of the core. The other is directly underneath, in contact with the core barrel liner. Sample thickness is usually measured by a vertical offset gauge. Fresh water was used to improve the acoustic contact between the core liner and the lower transducer. In highly indurated sediments, the measurements were done directly on core samples.

Shear Strength

Undrained shear strength (S_u) was determined perpendicular to bedding in fine-grained, plastic sediment by using the ODP motorized miniature vane shear device according to American Society for Testing and Materials (ASTM) D4648-87 guidelines (ASTM, 1987) and Boyce (1977). A 1.27-cm-diameter by 1.27-cm-high four-bladed vane was inserted into the split core and attached to a rotation sensor at each end of a coiled spring. The top of the spring was rotated at a constant rate of 89°/min until the calculated torque decreased or failed to increase with additional rotation.

The shear strength was calculated assuming that failure occurred on a right circular cylinder equal in surface area to the cylinder inscribed in the sediments by the vane during one continuous revolution.

The vane blade constant (K) was calculated from:

$$K = 2 / \{\pi \times D^2 \times H \times [1 + (D / 3H)]\},$$

where D and H are, respectively, the vane diameter and height in units of m, and K has units of m^{-3}. Torque (T) (N–m) was calculated from the measured differential spring rotation (Δ) and the spring calibration constant b:

$$T = b \times \Delta.$$

The undrained shear strength, in kPa, was then determined using:

$$S_u = T \times K.$$

Residual shear strength was recorded unless a significant post-peak decrease in stress did not occur with additional vane rotation. Errors associated with vane shear testing include (1) partial relief of pore pressure if the vane angular rotation rate is too slow for the sediment permeability, and (2) cracking of the sediment during vane rotation at higher shear strengths.

Electrical Resistivity

A four-probe configuration (Wenner spread) with two current and two potential electrodes systems was used to determine electrical resistivity. The electrodes were pushed approximately 2 mm into the split-core surface. Measurements were made with the probes aligned orthogonal to the core axis as well as parallel to it. An alternating current of 1 V was applied to the two outer electrodes, and the potential drop across the 0.15-mm spacing of the two inner electrodes was measured. The potential drop was converted to resistance by dividing by the instrument current. The resistance was then converted to resistivity by multiplying by the instrument cell constant. The cell constant is defined as the cross-sectional area divided by the distance between the two voltage electrodes. The cell constant was determined by measuring the resistance of a known fluid (seawater) at controlled temperatures.

Index Properties Measurements

Water content, wet-bulk density, dry-bulk density, and grain density were routinely determined using 10-cm^3 specimens collected from split cores. Porosity was calculated from these data under the assumption of a water salinity of 0.035 (see below). Immediately after collecting the samples, wet sediment mass and volume were measured. Dry sediment mass (M_d) and volume (V_d) were determined after the samples had dried for 24–36 hr at a temperature of 105° ± 5°C and cooled for 15 min in the desiccator.

Wet and dry sample mass were determined to a precision of ±0.01 g using a Scientech electronic balance. Where necessary, the sample mass was counterbalanced by a known mass to ensure that only mass differentials of up to 15 g were measured. The Quantachrome pentapycnometer determines volumes to an approximate precision of ±0.02 cm^3 based on the helium-displacement principle (see ASTM standard D 5550-94; ASTM, 1994). Four samples were run in conjunction with a reference volume as a blind to check for systematic error and calibrations. Calibrations were performed when needed and at least once per site.

Calculations of index properties were performed by the shipboard computer program "IP/4D." The correction factors and equations are similar to those employed during previous legs (e.g., Jansen et al., 1996). Six different parameters are calculated by the software. Five of these are determined in two ways: either by method B, which uses the wet total volume of the specimen, or by method C, which utilizes the dry volume of sediment. The tabulated data shown in the site chapters correspond to the following methods: wet-bulk density (wet method B), grain density (dry method C), dry density (wet method B), and porosity (wet method B). Water content is also tabulated, whereas the void ratio is calculated by the program but not tabulated in the site chapters.

The computer program corrected M_d and V_d to account for residual pore-water salt left behind by drying. The calculations were performed using the evaporated mass of pure water and an assumed salinity of 0.035, corresponding to a pore-water density of 1.024 g/cm^3 and a salt density of 2.257 g/cm^3. The formulas used for calculating the mass of salt, corrected mass of pore water, volume of pore water, mass of solids excluding salt, volume of salt, volume of solids excluding salt, water content, wet- and dry-bulk densities, grain density, porosity, and void ratio are listed in Shipboard Scientific Party (1996), and ASTM standard D2216-80 (ASTM, 1980).

Gammaspectral Scanning of Cretaceous/Tertiary Boundary Sections, Site 999 and Site 1000[3]

To identify the spectral gamma-ray signature of the Cretaceous/Tertiary (K/T) boundary sections penetrated during Leg 165, core sections containing the K/T boundary section of Hole 999B were measured by the natural gamma radiation detector on the shipboard multisensor track. The data were compared to the natural gamma-ray spectrometry (NGT) log for Hole 999B and correlated to the NGT log of Hole 1001A.

For Site 999, the spectral natural gamma radiation of the cores was measured between Sample 165-999B-59R-3, 76 cm, and 60R-1, 55 cm, at a 5-cm spacing and with counting times of 2 hr, and background counting times also of 2 hr. The routine MST data collection left no time for similar measurements of the cores from Site 1001. The gamma spectrum of the laboratory measurements was sampled over an energy interval from 0 to 3.1 MeV, distributed on 2048 channels. During post-cruise processing, K, U, and Th windows were defined as follows: K (1.36–1.56 MeV), U (1.61–1.86 MeV), and Th (2.32–2.97 MeV). The downhole logging data (see "Downhole Measurements" section, this chapter) are reported as K, U, and Th concentrations, as well as the total gamma radiation (SGR) and the computed K plus Th gamma radiation (CGR).

DOWNHOLE MEASUREMENTS

Introduction

The Lamont-Doherty Borehole Research Group (LDEO-BRG), in conjunction with Schlumberger Well Logging Services, provides the geophysical well logging aboard the *JOIDES Resolution.* Primarily designed for use in hydrocarbon exploration, logging tools have been adapted to meet ODP requirements and hole conditions. This includes the reduction of tool diameter to allow insertion into the 3.8-in drill-string bore.

Downhole logs are used to determine directly the physical, chemical, and structural properties of formations penetrated by drilling. Log data are collected continuously and interpretation of these continuous in situ measurements allow the formation's stratigraphic, lithologic, geophysical, and mineralogical characteristics to be quantified. When core recovery is incomplete, log data may serve as a proxy for physical properties and sedimentological data and permit the core to be placed in its proper stratigraphic position within the cored interval. Logs also complement discrete core measurements and offer additional advantage over core-based analyses in that they are rapidly collected and represent continuous in situ measurements. Geophysical well-logging is also used to aid in characterization of

[3]D.E. Paulsen, Department of Automation, Technical University of Denmark b. 322, DK-2800 Lyngby, Denmark; and I.L. Lind, Department of Geology and Geotechnical Engineering, Technical University of Denmark b. 204, DK-2800 Lyngby, Denmark.

sedimentary sequences when integrated with core and seismic reflection data.

On Leg 165, we used the Quad combination, the geochemical logging tool (GLT), the Formation MicroScanner (FMS), and the geological high-sensitivity magnetic tool (GHMT).

Well-Logging Operations

After coring was completed, the holes were flushed of sediment fill by circulating heavy viscous drilling fluid or seawater through the drill pipe to the mudline. The drilling assembly was pulled up to the upper logging point and then run down to the bottom of the hole again to condition the borehole for the logging program. Tool strings, comprised of one or more combinations of sensors, were then lowered downhole using a 7-conductor cable. A wireline heave-motion compensator (WHC) was employed to minimize the effect of ship's heave on the tool position in the borehole. The sensors continuously monitor the geophysical, geochemical, or structural properties of the formation, which are recorded by the Schlumberger MAXIS 500 or Cyber Service Unit (CSU) computers and then transferred to a Sun workstation and Macintosh computers for data display and interpretation. Logging data are typically recorded at 15-cm vertical intervals. The depths of investigation into the formation and the vertical resolution are sensor-dependent (Fig. 11).

Logging Tool Strings

Individual logging tools were combined in four different tool strings (Fig. 12) during Leg 165: the Quad combination (the seismic stratigraphy tool [NGT, LSS, DITE, TLT] and the lithoporosity tool [NGT, CNT-G, HLDT/CALI, TLT]), the geochemical combination (GLT), the Formation MicroScanner tool (FMS), and the geological high-sensitivity magnetic tool (GHMT). The Lamont-Doherty Earth Observatory (LDEO) temperature tool was attached to the base of the tool strings, except in the case of the FMS and the GHMT, to obtain downhole formation/fluid temperatures. The natural gamma-ray tool (NGT) was run as part of each tool string to correlate depths between different logging runs.

Logging Tools

A brief description of logging tools and their resolutions (Fig. 11) used during Leg 165 is given in the following sections. A detailed description of logging tool principles and applications is provided in Ellis (1987), Schlumberger (1989), and Timur and Toksöz (1985). The specifics of the standard wireline logging tools available to ODP are described in a recent Wireline Logging Services Guide (LDEO-BRG, 1994).

Natural Gamma-Ray Spectrometry Tool

The NGT measures the natural radioactivity of the formation using a NaI scintillation crystal mounted inside the tool. In formations, gamma-rays are emitted by the radioactive isotope ^{40}K and by the radioactive isotopes of the U and Th decay series. Measurements are analyzed by dividing the incident gamma-ray signature into five discrete energy windows that correspond to the main spectral peaks for each element. The total counts recorded in each window, for a specified depth in the well, are inverted to give the elemental abundances of K (wt%), U (ppm), and Th (ppm). The NGT also provides a measure of the total gamma-ray signature (SGR or [K + U + Th]) and a uranium-free measurement (CGR or [Th + K]). Values are recorded every 0.1524 m, and the vertical resolution of the NGT is roughly 46 cm (Fig. 11).

The natural gamma-ray measurement is commonly used to estimate the clay or shale content as there is a relatively high abundance of radioactive elements in the clay minerals. There are rock matrices,

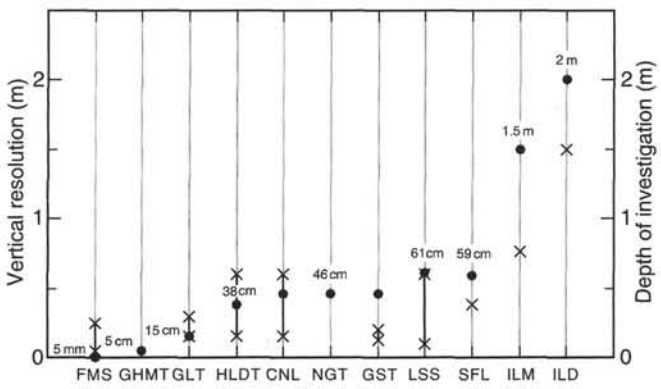

Figure 11. Vertical resolution (solid circles) and depth of investigation (crosses) of the Schlumberger logging tools deployed on Leg 165. The vertical resolution, or aperture, is the minimum depth interval for which a representative log measurement can be obtained. Modified from de Menocal et al. (1992). FMS = Formation MicroScanner, GHMT = geological high-sensitivity magnetic tool, GLT = geochemical logging tool, LDT = lithodensity tool, CNL = compensated neutron porosity log, NGT = natural gamma-ray tool, GST = gamma-ray spectroscopy tool, LSS = long-spaced sonic tool, SFL = shallow spherically focused resistivity tool, ILM = medium induction resistivity tool, and ILD = deep induction resistivity tool.

however, for which the radioactivity ranges from moderate to extremely high values because of the presence of volcanic ash, potassic feldspar, or other radioactive minerals. In addition, U/Th ratios from the NGT data are used as indicators of the organic carbon content; these ratios permit the determination of changes in the oxidation state of diagenetic minerals.

Phasor Dual Induction–Spherically Focused Resistivity Tool

The DITE–SFL provides three different measurements of electrical resistivity, each of which penetrates the formation to a different depth and has a different vertical resolution (Fig. 11). Values are recorded every 0.1524 m.

Water content and salinity are the most significant factors controlling the resistivity of rocks. Resistivity is therefore primarily related to the inverse square root of porosity (Archie, 1942). The other main factors influencing the resistivity of a formation include the concentration of hydrous and metallic minerals, the presence of hydrocarbons and gas hydrates, and the abundance, distribution, and geometry (tortuosity) of interconnected pore spaces.

Long-Spaced Sonic Tool (LSS)

The LSS measures the time required for acoustic waves to travel through the formation between an array of transmitters and receivers separated by vertical distances ranging from 0.91 to 3.66 m. It provides a direct measurement of acoustic velocity through sediments from the interval transit time measured, and is likely to yield measurements free from the effects of formation damage and enlarged borehole from drilling processes. Sound velocity is related to sediment porosity and lithification and/or compaction. In conjunction with density logs or core physical properties measurements, sonic logs can be used to compute synthetic seismograms. The vertical resolution of the LSS is 61 cm (Fig. 11).

High-Temperature Lithodensity Tool (HLDT)

The HLDT uses a ^{137}Ce gamma-ray source and measures the resulting gamma-ray flux at fixed distances from the source. Under

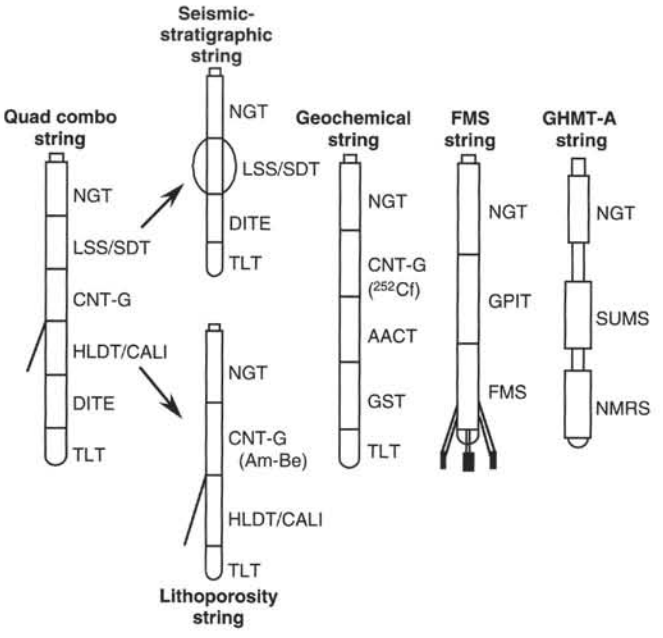

Figure 12. Schematic diagram of Schlumberger logging tool strings used on Leg 165. Tool strings are not drawn to scale. See text for an explanation of all abbreviations used.

normal operating conditions, the attenuation of gamma rays is primarily caused by Compton scattering (Dewan, 1983), which is related to electron density. Formation density is inferred from this gamma-ray flux by assuming a direct relationship between electron density and bulk density. This is normally valid because the ratio of atomic weight and the atomic number for most common rock-forming elements is constant (about 2:1).

The photoelectric absorption effect is used as an indicator of matrix lithology that is independent of porosity. Photoelectric absorption occurs at gamma-ray energies below which Compton scattering can usually occur (<100 keV). Besides being energy dependent, the probability of photoelectric absorption occurring is dependent on the atomic number of a formation (e.g., more sensitive to elements with higher atomic numbers). The magnitude of this measurement is therefore related to the abundance of the heavier "matrix" (mineral) portion of a formation, and for this reason it is almost entirely independent of porosity. The radioactive source and detector array is placed in a tool, which is pressed against the borehole wall by a strong spring arm. Excessive roughness of the hole will cause some drilling fluid to infiltrate between the detector and the formation. As a consequence, density readings can be artificially low. Approximate corrections can be applied using caliper data. The vertical resolution of the lithodensity tool is 38 cm (Fig. 11).

Compensated Neutron Porosity Tool (CNT-G)

Neutron logs are used principally for determination of formation porosity. The CNT-G uses a 16 Curie Am-Be chemical source, which bombards the formation and borehole with fast neutrons (4.5 MeV). Two pairs of sensors detect the number of neutrons (count rates) in the epithermal (0.1–100 eV) and thermal (<0.025 eV) energy ranges. The emitted neutrons interact elastically with the surrounding atoms and the greatest energy loss occurs with atoms of small capture cross-section, in particular hydrogen atoms (almost the same mass as one neutron). Thus, the slowing down and capture of the emitted neutrons is primarily controlled by the amount of hydrogen surrounding the tool. This hydrogen resides almost entirely in water molecules. Because this tool is very sensitive to hydrogen, it may provide the capability to detect occurrences of methane hydrates. The tool is designed to be run against the borehole wall. The CNT-G data, when used in the Quad combo (where the tool is not fully against the borehole wall) should be interpreted with caution. Poor tool contact with the borehole wall also leads to an overestimated formation porosity because, in addition to the borehole water, neutrons are strongly absorbed by Cl.

Both mineral-bound water (e.g., clay minerals) and water filling the pore space affect tool response, commonly leading to an overestimate of true porosity. Free-water content (porosity) is determined from the thermal neutron counts. Water that is structurally bound can be estimated by subtracting free water from the total water estimates. Neutron logs are also affected to some extent by matrix lithology of the formation. When the borehole fluid is gas-charged, this effect is reduced to a negligible level. These effects, however, and those caused by the amount and type of hydrocarbon, can be recognized and corrected for only if additional porosity information (i.e., from sonic and/or density logs) is available. The vertical resolution of the CNT-G is 55 cm.

Geochemical Logging Tool String

The geochemical tool string used on Leg 165 includes an NGT, an aluminum activation clay tool (AACT), a neutron porosity tool (CNT-G) that carries the ^{252}Cf neutron source for the AACT, and a gamma-ray spectrometry tool (GST) (Fig. 12). These tools use three separate modes of gamma-ray spectrometry for a comprehensive elemental analysis of the formation. Relative concentrations of Si, Ca, Fe, H, and Cl and wet weight percentages of K, U, Th, and Al are determined on board the ship. Shore-based processing is required to obtain dry weight percentages of the above elements in addition to Gd and Ti. Data from the GLT are acquired while logging uphole at 200 m/hr and can be obtained through the drill pipe, although the data are seriously degraded. Detailed information regarding gamma-ray spectrometry tools can be found in Hertzog et al. (1989), and onshore processing of the GLT data is described below.

Formation MicroScanner Tool (FMS)

The Formation MicroScanner (FMS) produces high-resolution images of the microresistivity character of the borehole wall that can be used for detailed sedimentological and structural interpretations (Ekstrom et al., 1986). The FMS tool contains 16 electrode buttons on four orthogonal pads that are pressed against the borehole wall. The electrode buttons are spaced 2.5 mm apart and are arranged in two vertically and diagonally offset rows of eight electrodes each. A focused electrical current flows between electrodes and the conductance of the borehole is measured. The conductance measurements are presented as microresistivity, although the FMS does not provide a direct, quantitative measurement of formation resistivity. Processing corrects the offset rows of electrodes to one level, providing a vertical resolution of 0.5 cm at a sampling interval of 0.25 cm (Fig. 11).

The FMS tool string includes a general purpose inclinometry tool (GPIT) that orients the data through the use of a three-axis accelerometer and magnetometer. The FMS tool string also includes an NGT to enable depth correlation of the FMS with other logging data. The raw FMS data are processed in real-time during logging to transform individual microresistivity traces into complete, oriented, variable intensity color images. Onboard image processing allowed production of full-color images at any scale. FMS images are used for detailed correlation of core and log depths, core orientation, mapping of fractures, faults, foliations, and formation structures including strike and dip of bedding. In addition, the FMS can provide information on the orientation of the in situ stress field by imaging the directions of borehole breakouts, and by providing precise measurements of borehole diameter in two orthogonal directions.

Lamont-Doherty Temperature Tool

The LDEO temperature logging tool (TLT) is a self-contained tool that can be attached to the base of any of the Schlumberger tool strings. Data from two thermistors and a pressure transducer are collected at a predetermined rate of one sample per second and stored within the tool. A fast-response, lower accuracy thermistor is able to detect sudden temperature excursions caused by fluid flow from the formation. A slow-response, higher accuracy thermistor can be used to estimate borehole fluid temperature. Data are recorded as a function of time, with conversion to depth based on pressure recordings from the pressure transducer and on the synchronized time-depth record of the wireline cable. The TLT measures the borehole water temperature, not the true formation temperature; it is common to observe gradual borehole warming (thermal rebound) as logging proceeds. The TLT data do not record the true temperature gradient and, therefore, should not be used in heat-flow calculations. The TLT data are useful for the calculation of borehole fluid resistivities for log porosity estimates and for the calibration of FMS data using resistivities measured by the spherically focused resistivity tool (SFL).

Geological High-Sensitivity Magnetic Tool String

The GHMT-A was developed jointly by Schlumberger, two French government research institutions (CEA-LETI and CNRS-ENS), and an oil company (TOTAL). The tools were designed and constructed by a branch of the French Atomic Energy Commission (CEA-LETI), which also developed the analysis software.

The GHMT-A comprises a high-sensitivity total magnetic field sensor (Nuclear Magnetic Resonance Sonde [NMRS]) coupled with a magnetic susceptibility sensor (Susceptibility Magnetic Sonde [SUMS]), which are used to detect borehole magnetic polarity transitions and susceptibility variations. The NMRS measures the frequency of proton precession between a calibrated applied polarizing field and Earth's magnetic field that is proportional to the total field intensity of the earth. The tool has an average precision of 0.5 nT and a sensitivity of about 10^{-2} nT. The SUMS measures mutual inductance caused by the surrounding borehole lithology using a transmitter coil and a receiver coil separated as a two-coil induction sonde. The operating frequency is about 200 Hz. The precision between duplicate runs is generally better than 3 ppm (3×10^{-6} SI), and the sensitivity of the sonde is almost 10^{-6} units. Data are recorded every 5 cm with a vertical resolution of 5 cm (Fig. 11).

Magnetic induction B in a borehole depends on position p and time t (Pozzi et al., 1988) with:

$$B(p,t) = Br(p) + Ba(p) + Bf(p) + Bt(p,t),$$

where $Br(p)$ is the dipolar Earth's field and $Ba(p)$ is the anomaly field related to large-scale heterogeneities in susceptibility or in magnetic remanence. In the absence of such heterogeneities, the spatial variation of Br with depth is linear. $Bf(p)$ is the induction caused by magnetization (induced and remanent) of the sediments around the borehole; it can easily be separated from $Br(p)$ and $Ba(p)$ by subtracting the Earth's magnetic field gradient and by applying a high-pass filter. $Bt(p,t)$ is time dependent and represents the induction caused by transient variations of the Earth's magnetic field. At sea, the time-dependent component can be estimated by repeat sections. To obtain direct magnetostratigraphy from $Bf(p)$, the susceptibility and the total field measurements are combined to discriminate the induced and remanent magnetizations. Specifications of the probes, such as impulse response, calibration ratio, and geomagnetic location of the hole, are used to calculate the susceptibility effect on the scalar total field magnetometer. From these data, the polarity of the scalar remanent magnetization can be calculated (Pozzi et al., 1993).

Log Data Quality

Log data quality may be seriously degraded by rapid changes in the hole diameter and in sections where the borehole diameter is greatly increased or washed out. The result of these effects is to impair logging by causing "bridging" or "tool sticking" and to increase the fluid volume between the formation and the logging tool. Deep investigation devices such as resistivity and velocity tools are least sensitive to borehole effects. Nuclear measurements (density, neutron porosity, and both natural and induced spectral gamma ray) are more sensitive because of their shallower depth of investigation as well as the effect of increased drill fluid volume on neutron and gamma-ray attenuation. Corrections can be applied to the original data to reduce these effects, but they cannot account for very large washouts.

Using the NGT during each logging run allows the depth to be correlated between logging runs. However, logs from different tool strings may still have minor depth mismatches caused either by cable stretch or ship heave during recording. Furthermore, to aid in depth correlation between tool strings, and to collect an accurate depth to bottom measurement, the Quad combo tool string was pulled to seafloor depth at each site. Again, using the NGT, an accurate mudline measurement was acquired. Small errors in depth matching can impair the multilog analyses in zones of rapidly varying lithology.

Shore-Based Log Processing

Processing, quality control, and display of the logging data were performed at each of the four holes logged during Leg 165 by the Borehole Research Group (BRG) at LDEO, the Institut Mediterraneen de Technologie, and Schlumberger GeoQuest using Schlumberger "Logos" software and additional programs developed by members of the BRG. Displays of most of these processed data appear with accompanying text at the end of the appropriate site chapters in this volume. Files of all processed logs (including FMS, dipmeter, temperature data, high-resolution density and neutron data, sonic waveforms, and magnetic data not shown in printed form) and explanatory text are included on CD-ROM in the back pocket of this volume; a directory of CD-ROM contents is found at the front of this volume.

Shore-based processing of data from each hole consisted of (1) depth adjustments of all logs to a common measurement below the seafloor, (2) corrections specific to certain tools, and (3) quality control and rejection of unrealistic values.

The depth-shifting procedure is based on an interactive, graphical depth-match program that allows the processor to correlate logs visually and to define appropriate shifts. The reference log and the log to be adjusted in depth are displayed side by side on a screen, and vectors connect the two at positions chosen by the user. The total gamma-ray curve (SGR) from the NGT tool run on each logging string was used in most cases to correlate the logging runs. In general, the reference curve is chosen on the basis of constant, low cable tension and high cable speed (tools run at faster speeds are less likely to stick and are less susceptible to data degradation caused by ship heave). Other factors, however, such as the length of the logged interval, the presence of a bottom-hole assembly, and the statistical quality of the collected data (better statistics are obtained at lower logging speeds) are also considered in the selection. A list of the amount of differential depth shifts applied at each hole is available upon request to BRG (L-DEO).

Specific tool corrections were performed on the gamma-ray data to account for changes in borehole size and for the composition of the drilling fluid. Processing techniques unique to the AACT and GST tools of the geochemical string are described in detail below.

Quality control was performed by cross-correlation of all logging data. If the data processor concluded that individual log measurements represented unrealistic values, the choices were either to dis-

card the data outright and substitute the null value of "–999.25," or identify a specific depth interval containing suspect values that must be used with caution. The latter are noted in the text that accompanies all processed log displays. Quality control of the acoustic data was based on discarding any of the four independent transit time measurements that were negative or that fell outside a range of reasonable values selected by the processor.

In addition to the standard 15.24-cm sampling rate, bulk density and neutron data were recorded at a sampling rate of 2.54 and 5.08 cm, respectively. The enhanced bulk density curve is the result of a Schlumberger-enhanced processing technique performed on the MAXIS system on board. Although short-spacing data are smoothed to match long-spacing data in normal processing, in enhanced processing this is reversed. In a situation where there is good contact between the HLDT pad and the borehole wall (low-density correction), the results are improved because the short-spacing data have better vertical resolution.

Locally, some intervals of log data appeared unreliable (usually because of poor hole conditions) and were not processed. In general, a large (>12 in) and/or irregular borehole affects most recordings, particularly those that require eccentralization (HLDT) and a good contact with the borehole wall. Hole deviation can also degrade the data; the FMS, for example, is not designed to be run in holes that are more than 10° off the vertical, as the tool weight might cause the caliper to close.

The Geological Magnetic Tool collected data at two different sampling rates: the standard 0.1524 m rate, and a rate of 0.0508 m. Both data sets are routinely depth shifted to the reference run and to the seafloor.

Geochemical Tool String[4]

Geochemical logging was conducted at Sites 998 and 999. At Hole 998B, located on the Cayman Rise, a complete suite of logs, including conventional, geochemical, Formation MicroScanner, and geologic magnetic tools, was recorded. The quality of the data is generally good, with the exception of the neutron porosity tool, which was affected by an intermittent detector problem and borehole conditions.

Hole 999B, which penetrated 1066.4 mbsf on the Kogi Rise, in the Colombian Basin, was logged with the conventional, geochemical, and Formation MicroScanner tools. The data were generally good at this site as well, with the exception of the lithodensity tool; instability of the long-spacing detector, possibly because of borehole conditions, caused frequent spikes in the recording.

The geochemical logging tool string consists of four logging tools: the natural gamma-ray tool (NGT), the compensated neutron tool (CNT), the aluminum activation clay tool (AACT), and the gamma-ray spectrometry tool (GST; Fig. 13). The natural gamma-ray tool is located at the top of the tool string, so that it can measure the naturally occurring radio nuclides (Th, U, and K) before the formation is irradiated by the nuclear sources contained in the other tools. The compensated neutron tool, located below the natural gamma-ray tool, carries low-energy californium-252 (^{252}Cf) to activate the Al atoms in the formation. The aluminum activation clay tool, a modified NGT, is located below the ^{252}Cf source, measuring the activated gamma rays in the formation. By combining the AACT measurement with the previous NGT measurement, the background radiation is subtracted out and a reading of formation Al is obtained (Scott and Smith, 1973). The gamma-ray spectrometry tool, at the base of the string, carries a pulsed neutron generator to bombard the borehole and formation and a NaI(Tl) scintillation detector, which measures the spectrum of gamma rays generated by neutron-capture reactions.

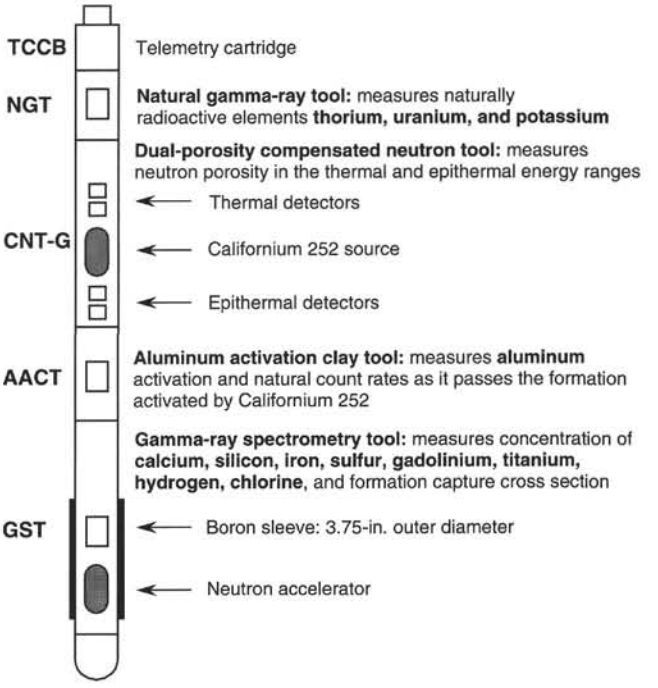

Figure 13. Schematic drawing of the Schlumberger geochemical logging tool string used in the Ocean Drilling Program.

Because each of the elements in the formation is characterized by a unique spectral signature, it is possible to derive the contribution (or yield) of each of the major elements silicon (Si), iron (Fe), calcium (Ca), titanium (Ti), sulfur (S), gadolinium (Gd), and potassium (K) to the measured spectrum and, in turn, to estimate its abundance in the formation. The GST also measures the presence of hydrogen (H) and chlorine (Cl) in the borehole and formation; but the signal for these elements is almost entirely caused by seawater in the borehole and is, therefore, of little value.

The only major rock-forming elements not measured by the geochemical tool string are magnesium (Mg) and sodium (Na); the neutron-capture cross-sections of these elements are too small relative to their typical abundance for the tool string to detect them. A rough estimate of Mg + Na can be made by using the photoelectric factor (PEF), measured by the lithodensity tool. This measured PEF is compared with a calculated PEF (a summation of the PEF from all of the measured elements). The separation between the measured and calculated PEF is, in theory, attributable to any element left over in the formation (i.e., Mg and Na). Further explanation of this technique is found in Hertzog (1987). The Mg + Na calculation was not performed for any of the logs discussed here because of the high variance in the data caused by the poor hole conditions.

Data Reduction

The well log data from the Schlumberger tools are transmitted digitally up a wireline and are recorded on the *JOIDES Resolution* in the Schlumberger Cyber Service Unit (CSU). The results from the CSU are made available as "field logs" for initial, shipboard interpretation. Subsequent reprocessing is necessary to correct the data for the effects of fluids added to the well, logging speed, and pipe interference. Processing of the spectrometry data is required to transform the relative elemental yields into oxide weight fractions.

The processing is performed with a set of log interpretation programs written by Schlumberger that have been slightly modified to account for the lithologies and hole conditions encountered in ODP holes. The processing steps are summarized below.

[4]Performed by Elizabeth Pratson at Schlumberger GeoQuest, 6090 Greenwood Plaza Englewood, CO 80111, U.S.A.

Step 1: Reconstruction of Relative Elemental Yields from Recorded Spectral Data

The first processing step uses a weighted least-squares method to compare the measured spectra from the geochemical spectrometry tool with a series of standard spectra in order to determine the relative contribution (or yield) of each element. Whereas six elemental standards (Si, Fe, Ca, S, Cl, and H) are used to produce the shipboard yields, three additional standards (Ti, Gd, and K) can be included in the shore-based processing to improve the fit of the spectral standards to the measured spectra (Grau and Schweitzer, 1989). Although these additional elements often appear in the formation in very low concentrations, they can make a large contribution to the measured spectra, because they have large neutron-capture cross-sections. For example, the capture cross-section of Gd is 49,000 barns; that of Si is 0.16 barns (Hertzog et al., 1987). Gd is included, therefore, in the calculation of a best fit between the measured and the standard spectra. This best-fit analysis was done for the elements in each of the logged holes to include spectral standards for Si, Ca, Fe, Ti, Gd, S, K, H, and Cl in both holes logged with the geochemical tool; however, K was omitted in Hole 998B as it added noise to the reconstructed yields.

Step 2: Depth Shifting

The second step in log processing involves depth shifting the logging runs to a chosen reference run. A total gamma-ray curve (from the NGT, which is run on each tool string) is usually chosen as a reference curve, based on cable tension (the logging run with the least amount of cable sticking) and cable speed (tools run at faster speeds are less likely to stick). For Hole 998B, the reference NGT run was taken from the geophysical (DIT/SDT/HLDT/CNTG/NGT) run. For Hole 999B, the NGT curve on the geochemical logging tool itself was used as the reference curve, so no depth shifting was necessary at this stage.

Step 3: Calculation of Total Radioactivity and Th, U, and K Concentrations

The third processing routine calculates the total natural gamma radiation in the formation as well as concentrations of Th, U, and K, using the counts in five spectral windows from the natural gamma-ray tool (Lock and Hoyer, 1971). This resembles shipboard processing, except that corrections for hole-size changes are made in the shore-based processing of these curves. A Kalman filter (Ruckebusch, 1983) is applied to minimize the statistical uncertainties in the logs, which would otherwise create erroneous negative readings and anti-correlation (especially between Th and U). At each depth level calculations and corrections also were performed for K contained in the mud. This K correction is particularly useful where KCl is routinely added to the hole; however, because of dispersion it is difficult to know exactly how much K is in the borehole. The outputs of this program are K (wet wt%), U (ppm), and Th (ppm), along with a total gamma-ray curve and a computed gamma-ray curve (total gamma ray minus U contribution). They are displayed as a function of depth in the log summary figures at the end of the relevant site chapter (this volume).

Step 4: Calculation of Al Concentration

The fourth processing routine calculates an Al curve using four energy windows, while concurrently correct for natural activity, borehole fluid neutron-capture cross-section, formation neutron-capture cross-section, formation slowing-down length, and borehole size. Porosity and density logs are needed in this routine to convert the wet weight percent K and Al curves to dry weight percent.

A correction is also made for Si interference with Al; the 252Cf source activates the Si, producing the aluminum isotope, Al28 (Hertzog et al., 1987). The program uses the Si yield from the gamma-ray spectrometry tool to determine the Si background correction. The program outputs dry weight percentages of Al and K, which are used in the calculation and normalization of the remaining elements.

Step 5: Normalization of Elemental Yields from the GST to Calculate the Elemental Weight Fractions

This routine combines the dry weight percentages of Al and K with the reconstructed yields to obtain dry weight percentages of the GST elements using the relationship:

$$W_i = F\, Y_i / S_i\,, \tag{1}$$

where W_i = dry weight percentage of the i-th element, F = normalization factor determined at each depth interval, Y_i = relative elemental yield for the i-th element, and S_i = relative weight percentage (spectral) sensitivity of the i-th element.

The normalization factor, F, is a calibration factor determined at each depth from a closure argument to account for the number of neutrons captured by a specific concentration of rock elements. Because the sum of oxides in a rock is 100%, F is given by

$$F\,(\Sigma\, X_i\, Y_i / S_i) + X_K\, W_K + X_{Al}\, W_{Al} = 100.0, \tag{2}$$

where X_i = factor for the element to oxide (or carbonate) conversion. X_K = factor for the conversion of K to K_2O (1.205), X_{Al} = factor for the conversion of Al to Al_2O_3 (1.899), W_K = dry weight percentage of K determined from natural activity, and W_{Al} = dry weight percentage of Al determined from the activation measurement.

The sensitivity factor, S_i, is a tool constant measured in the laboratory, that depends on the capture cross-section, gamma-ray production, and detection probabilities of each element measured by the GST (Hertzog et al., 1987).

The factors X_i are simply element-to-oxide (or carbonate, sulfate, etc.) conversion coefficients and effectively include the O, C, or S bound with each element. In processing the GLT data, the correct choice of X_i is important in the closure algorithm described above and requires some geological input. In most lithologies, the elements measured by the tool occur in silicates where the compositions can be expressed completely as oxides.

With carbonate or carbonate-rich lithologies, the measured calcium is more likely to be present as $CaCO_3$ (XCa = 2.497) than as the oxide (CaO; XCa = 1.399). A good indication of the choice of calcium conversion factors can often be gained from shipboard XRD and $CaCO_3$ measurements that estimate acid-liberated $CaCO_3$. In the absence of suitable shipboard data, a rough rule of thumb is generally used such that if elemental Ca is below 6%, then all Ca is assumed to be in silicate; above 12%, in carbonate. Calcium concentrations between these figures are converted using linear interpolation. During Leg 165, a value of 2.497 was used in the carbonate-dominated sediments of Holes 998B and 999B.

Step 6: Calculation of Oxide Percentages

This routine converts the elemental weight percentages into oxide percentages by multiplying each by its associated oxide factor, as shown in Table 8. The results are displayed as a function of depth in the log summary figures at the end of the relevant site chapter (this volume); the calcium carbonate measurements performed on board for all holes are also displayed.

Step 7: Calculation of Error Logs

The seventh and final step in processing is the calculation of the statistical uncertainty of each element, using methods described by Grau et al. (1990) and Schweitzer et al. (1988). This error is strongly related to the normalization factor, F, which is calculated at each depth level. The normalization factor as well as statistical uncertainties are displayed as a function of depth in the log summary figures at

Table 8. Oxide factors used in normalizing elements to 100% and converting elements to oxides.

Element	Oxide/carbonate	Conversion factor
Si	SiO_2	2.139
Ca	$CaCO_3$	2.497 (for Holes 998B and 999B)
Ca	CaO-$CaCO_3$	1.399–2.497
Fe	FeO*	1.358
K	K_2O	1.205
Ti	TiO_2	1.668
Al	Al_2O_3	1.889

the end of the relevant site chapter (this volume). A lower normalization factor represents better counting statistics and therefore higher quality data.

UNDERWAY GEOPHYSICS AND PRE-SITE SEISMIC SURVEYS

Introduction

Site selection for Leg 165 was based on seismic, bathymetric, coring, and dredge data collected during several separate surveys. Data from each of these surveys are described in the "Seismic Stratigraphy" section of each site chapter. Underway geophysical data, excluding single-channel seismic (SCS) surveys, were collected as we approached all sites. The SCS data were only collected during the approach to Site 999. Onboard instrumentation used included precision echo-sounders (3.5 and 12 kHz), a magnetometer, a seismic reflection acquisition system, and global positioning satellite navigation systems.

Instrumentation

Navigation

The Global Positioning System (GPS) was used throughout Leg 165. Three GPS systems were available for operation, with output provided to the underway geophysics laboratory. Two of these were new differential GPS systems (DGPS), Omnistar Model 6300A-G, providing coverage to the continental United States and to parts of Canada and northern Mexico. Because of an equipment malfunction, only one of these systems could acquire DGPS, and it only provided DGPS data up until shortly after leaving Site 998. The accuracy of DGPS appeared superior to regular GPS at port in Miami but seemed to degrade as we reached beyond the perimeters of the coverage area. After the DGPS degraded, the GPS from one of the Omnistar systems was used as the primary navigation device throughout the leg. The third GPS system (available but not used) was the much older Magnavox Model MX1107 receiver.

GPS fixes were available continuously and were recorded at approximately 1-s intervals. Event data were recorded at 60-s intervals on site and in transit, and at the selected seismic gun firing rate (12 s) during the single-channel seismic survey at Site 999.

Navigation data were logged by the WINFROG software system, mounted on a dedicated PC in the underway geophysics laboratory. Subsequent processing and display of navigation data were performed using the Generic Mapping Tool (GMT) software package (Wessel and Smith, 1991) on shipboard Unix workstations.

Echo-Sounders

Two low-frequency echo-sounders (precision depth recorders; PDR), running at 3.5 and 12 kHz, respectively, were used to acquire bathymetric data as well as high-resolution reflection records of the uppermost sediment layers. Data from both systems were recorded on Raytheon Model 1807M analog line scanning recorders. Both the 3.5- and 12-kHz systems used a Raytheon CESP III Correlator Echo-Sounder Processor driven by a Raytheon PTR105B transceiver with a 2-kw sonar transmitter. The 3.5- and 12-kHz PDRs each used a single EDO type 323c transducer. The transducers were mounted in a sonar dome on the hull 45 m forward of the drill floor. This location was chosen to reduce ship-generated noise and signal attenuation from aeration beneath the hull. Both recorders were annotated automatically at fixed intervals, usually every 0.5 hr. Depth readings were taken manually every 5 min and entered into an EXCEL spreadsheet.

Seismic Reflection Profiling

Available shipboard seismic sources for underway seismic profiling consisted of Seismic Systems, Inc., water guns with volumes that ranged from 80 to 200 in^3. Two 200-in^3 water guns were used to image basement and approximately 1400 m of overlying sediment at Site 999.

The seismic data were recorded using a single-channel Teledyne Model 178 hydrophone streamer with a 100-m-long active section containing 60 hydrophones, a 15-m-long "stretch" section, and a 488-m lead section. The head of the streamer was positioned approximately 503 m behind the ship. During approach operations at Site 999, one 200-in^3 water gun was initially deployed along with the port streamer, but the signal was unusually noisy and low amplitude. The port streamer was reeled in and the starboard streamer was deployed along with a second 200-in^3 water gun. The signal was somewhat improved but still poor in quality. The guns and streamer were both towed at 12–18 m depth. Ship's speed averaged 4.6 kt during the initial approach to the site on a 135° course and averaged 6.7 kt during a second site crossing on a 270° course (see Fig. 2, "Seismic Stratigraphy" section, "Site 999" chapter). The two synchronized water gun sources operated at 1900–2000 psi and were triggered from the WINFROG navigation system at a shot interval of 12 s, equivalent to 31 m at 5 kt. The guns were towed approximately 25 m astern and 14 m apart. Analog data were recorded on two Raytheon Model 1807M recorders ("Analog-1" and "Analog-2"), displaying scan intervals appropriate for water depth and sediment thickness at each site (e.g., 3–6 s at Site 999). Signals received by Analog-1 were filtered from 25 to 90 Hz throughout each seismic survey. Analog-2 signals were filtered at various band-pass ranges between 20 and 150 Hz. Krohn-Hite Model 3550 analog filters were used to filter signals to both recorders.

The seismic data from each shot were sampled every 1 ms for 8 s and were digitally recorded on a Sun Sparcstation 10 in SEGY format, using the "a2d" acquisition package after application of an anti-aliasing filter with a corner frequency at 250 Hz. Seismic data were copied to 4- and 8-mm digital audio tapes after the site survey. Seismic data were processed using the SIOSEIS software package (Paul Henkart, Scripps Institute of Oceanography), and displayed on a HP 650C "Design Jet" plotter. Processing of SCS water gun data acquired during Leg 165 included water bottom mute, band-pass filter (20–80 Hz), weighted 3-trace running mix, and automatic gain control (AGC), using a 500-ms window and removing every other trace ("Seismic Stratigraphy" section, "Site 999" chapter, this volume).

Magnetometer

Total intensity measurements of the Earth's magnetic field were obtained with a Geometrics Model G-886 proton precession magnetometer towed approximately 500 m astern. Magnetic data were recorded throughout the leg, generally during transits and during the site surveys. The exceptions during transit were caused by either shallow water or shipping lane traffic. Magnetic data were recorded at 1-min intervals during transit and every 12 s during SCS acquisition on navigation files produced by WINFROG navigation software.

Pre-Site Surveys

The type, grid density, and data quality of available pre-cruise seismic site survey data were quite variable from site to site. In addition, some survey lines were acquired before the availability of GPS

coverage (Site 999) or with only partial GPS coverage (Site 1002); consequently, these had less reliable navigation data. Individual site surveys are described in the following paragraphs.

Maurice Ewing *Cruise EW9417*

A 2.5-day site survey, linked to the transit from Panama to Tampa of the *Maurice Ewing* (EW9417, 27 November–8 December 1994) was funded by JOI-USSAC to survey several of the sites proposed for Leg 165 (Sites 998, 999, 1000, and 1001) (A.W. Droxler, unpubl. report, 1995; Droxler et al., 1995). The seismic source used during EW9417 consisted of two 80-in^3 SSI water guns fired every 10 s. Seismic data were recorded by means of a single-channel streamer and digitized at a 1-ms sampling interval with the Elics/Delph2 system of Rice University and the Digicon system on board the *Maurice Ewing*. Ship speed was held at 6 kt during seismic acquisition and GPS navigation was available throughout the transit and survey.

The EW9417 expedition collected a grid of digital SCS, Hydrosweep swath bathymetric, analog 3.5-kHz, gravity, and magnetic data over Site 998 (Cayman Rise). The 272-km survey grid consists of four northwest/southeast lines, ranging in length from 16 to 42 km, and four southwest/northeast cross-lines, ranging in length from 16 to 54 km ("Seismic Stratigraphy" section, "Site 998" chapter, this volume). The 5.4-km spacing between the lines allowed full bathymetric coverage with the Hydrosweep.

Site 999 (Colombian Basin, Kogi Rise) was partially surveyed during the transit of EW9417. Hydrosweep bathymetric (approximately 6 km in width) and analog 3.5-kHz data were collected along a single 80-km-long line, which was coincident with the existing multichannel seismic line (*Ida Green* 2901 Line CT 1-12a) across the proposed site.

Site 1000 (Pedro Channel, northern Nicaraguan Rise) was surveyed with three passes of the Hydrosweep, each corresponding to a 2.7-km swath width, and analog 3.5-kHz profiles. In addition, analog 3.5-kHz profiles were obtained along an existing SCS line (*Cape Hatteras* 9204-30), and at close proximity to Site 1000, along an existing east-west cross SCS line (*Cape Hatteras* 9204-05).

The Site 1001 area (Hess Escarpment, lower Nicaraguan Rise) was surveyed with a grid of digital SCS, Hydrosweep swath bathymetry, analog 3.5-kHz, gravity, and magnetic data. The 335-km grid consists of six dip lines and two strike lines relative to the northeast-trending Hess Escarpment, providing full coverage in terms of swath bathymetry in two southwest and northeast areas linked by the strike lines. The middle dip line (Line EW9417-02) in the southwest survey area is coincident with an existing MCS line (CASIS MCS Line C0-01), and the middle dip line (Line EW9417-08) in the northeast survey area and one strike line (Line EW9417-10) cross DSDP Site 152, providing ties to Site 1001, located farther southeast on Line EW9417-10 ("Seismic Stratigraphy" section, "Site 1001" chapter, this volume).

Ida Green *Cruise IG2901*

Cruise IG2901 is one of several MCS expeditions throughout the Caribbean Sea conducted by the University of Texas Institute for Geophysics (UTIG) from 1975 to 1978 aboard the *Ida Green* (Bowland and Rosencrantz, 1988; Bowland, 1993). Site 999 is located approximately 800 m east of shotpoint 4780 of IG2901 MCS line CT1-12a, which was obtained on 28/29 May 1978. Navigation for this line consisted of transit satellite and dead reckoning. The position of Site 999 determined by GPS lies within the error of this 1978 vintage navigation. Line CT1-12 continues for hundreds of kilometers to the southwest of Site 999, crossing the Mono Rise and the Costa Rican Fan and continuing to the northeast of Site 999 into the eastern Colombian Basin (see Fig. 2, "Seismic Stratigraphy" section, "Site 999" chapter, this volume). The seismic source used during the acquisition of line CT1-12a consisted of two 1500-in^3 Bolt Inc. air guns fired at approximately 116-m intervals. Seismic data were received using an array of 24 hydrophone groups each 100 m in length. The maximum hydrophone group offset ranged from 2405 to 2638 m. Data were digitally recorded at a 4-ms sampling interval. This single MCS line provided the primary information for site location. Interval velocities based on the average of 48 to 50 semblance-type velocity analyses at 5-km intervals along CT1-12 were reported in Bowland (1993) and were used to estimate sediment thicknesses before drilling began.

Data processing included demultiplexing, trace editing, common-depth-point (CDP) sorting, semblance velocity analyses (spaced at 5-km intervals), 12-fold stacking, band-pass filtering (5–50 Hz), and application of an AGC with a 500-ms window. The IG2901 data displayed in this volume consist of 12-fold stack data provided by UTIG with band-pass filters (5–50 Hz) and 500-ms AGC applied using SIOSEIS software and the HP 650C plotter aboard the *JOIDES Resolution.*

Maurice Ewing *Cruise EW9501*

A regional geophysical survey of the Venezuelan Basin, Beata Ridge, and Hess Escarpment was conducted aboard the *Maurice Ewing* expedition EW9501 during February and March 1995 (Diebold et al., 1995). The EW9501 cruise collected 5700 km of MCS along with coincident magnetic, gravity, and Hydrosweep swath bathymetric data. Wide-angle reflection and refraction data were also recorded using expendable sonobuoys deployed at regular intervals along track. The majority of MCS coverage was in the Venezuelan Basin and on the Beata Ridge; however, two lines (1329 and 1330) crossed the Hess Escarpment within 3 and 5 km of Site 1001 and DSDP Site 152, respectively, and intersected SCS lines collected during EW9417.

The seismic source consisted of a 20 air gun tuned array with a total volume of 8470 in^3. This configuration produced a powerful broadband source (deep penetration and high resolution), which provided additional constraints for locating Site 1001. Only SCS profiles (near-channel trace from the MCS streamer) were available during Leg 165 ("Seismic Stratigraphy" section, "Site 1001" chapter, this volume). Complete processing of these lines will occur on shore after the completion of Leg 165.

Cape Hatteras *Cruise CH9204*

The seismic survey in Pedro Channel, where Site 1000 (NR1/2) is located, consists of 2200 km (32 lines) of digital, high-resolution SCS data collected in Spring 1992 with the *Cape Hatteras* (Droxler et al., 1992). The profiles were shot using an SSI 80-in^3 GI gun as a source fired at between 7 and 10 s at an average speed of 5.5 kt. Both analog and digital data were recorded. The digital data were recorded using the Masscomp aboard the *Cape Hatteras* as well as the Elics/Delph1 system of Rice University at a sampling rate of 0.5 ms. Profile record lengths are 3 s plus deep-water delay, and water bottom penetration ranges from minimal on the banks to 2 s within the basins. Navigation was based on GPS, which was available continuously through the duration of the cruise. Over 2200 km of 3.5-kHz profiles were acquired using a hull-mounted array of 9 Raytheon TR-109 kHz transducers and Edo 248E transceivers. The 3.5-kHz analog data were recorded along the same lines as the single-channel air gun data and were integrated into the existing bathymetric data to revise the general bathymetry of Pedro Channel (see "Seismic Stratigraphy" section, "Site 1000" chapter, this volume). Site 1000 is located on one north/south high-resolution seismic line (Line CH9204-30) and in close proximity to an east-west cross line (Line CH9204-32).

In addition to the geophysical survey, 20 piston cores were collected in Pedro Channel. The cores, ranging in length from 397 to 1126 cm, are kept in the cold storage facility of Rice University (at 4°C). Finally, 14 dredge sites were occupied and nine dredges came back with freshly broken rock pieces consisting of grainstone, chalk, or well-lithified limestone.

Thomas Washington *PLUME Expedition Leg 7 (PLUME-7)*

Site survey data for the Cariaco Basin drilling effort were collected on Leg 7 of the PLUME Expedition (June 1990) using the *Thomas Washington.* Although primarily a sediment coring cruise, a detailed grid (5-km line spacing) of high-resolution SCS, analog 3.5-kHz, magnetic, and gravity data was collected over the central saddle and northern slopes of the two Cariaco sub-basins. Using an 80-in^3 water gun as the source signal, SCS data were digitally recorded during the cruise at a 1-ms sampling rate with an anti-aliasing filter of 250 Hz for post-cruise processing. Site 1002 (proposed Site CB-1A) is essentially a redrilling of DSDP Site 147, and it falls near the crossing of east-west PLUME-7 line W1-X1 and north-south line J1-K1 ("Seismic Stratigraphy" section, "Site 1002" chapter, this volume).

REFERENCES

Archie, G.E., 1942. The electrical resistivity log as an aid in determining some reservoir characteristics. *J. Pet. Technol.,* 5:1–8.

ASTM, 1980. Standard method for laboratory determination of water (moisture) content of soil, rock and soil-aggregate mixtures. In *Annual Book of ASTM Standards:* Philadelphia (Am. Soc. Testing and Mater.).

————, 1987. Standard test method for laboratory miniature vane shear test for saturated fine-grained clayey soil. In *Annual Book of ASTM Standards* (Vol. 04.08): Philadelphia (Am. Soc. Testing and Mater.).

————, 1994. Standard test method for specific gravity of soil solids by gas pycnometer. In *Annual Book of ASTM Standards* (Vol. 04.08): Philadelphia (Am. Soc. Testing and Mater.).

Aubry, M.-P., 1984. *Handbook of Cenozoic Calcareous Nannoplankton* (Book 1): *Ortholithae (Discoasters):* New York (Micropaleontology Press).

————, 1988. *Handbook of Calcareous Nannoplankton* (Book 2): *Ortholithae (Catinasters, Ceratoliths, Rhabdoliths):* New York (Micropaleontology Press).

————, 1989. *Handbook of Cenozoic Calcareous Nannoplankton* (Book 3): *Ortholithae (Pentaliths and Others). Heliolithae (Fasciculiths, Sphenoliths, and Others):* New York (Micropaleontology Press).

————, 1990. *Handbook of Cenozoic Calcareous Nannoplankton* (Book 4): *Heliolithae (Helicoliths, Cribriliths, Lopadoliths, and Others):* New York (Micropaleontology Press).

Backman, J., and Raffi, I., in press. Calibration of Miocene nannofossil events to orbitally tuned cyclostratigraphies from Ceara Rise. *In* Curry, W.B., Shackleton, N.J., Richter, C., Bralower, T.J., et al., *Proc. ODP, Sci. Results,* 154: College Station, TX (Ocean Drilling Program).

Backman, J., Schneider, D.A., Rio, D., and Okada, H., 1990. Neogene low-latitude magnetostratigraphy from Site 710 and revised age estimates of Miocene nannofossil datum events. *In* Duncan, R.A., Backman, J., Peterson, L.C., et al., *Proc. ODP, Sci. Results,* 115: College Station, TX (Ocean Drilling Program), 271–276.

Backman, J., and Shackleton, N.J., 1983. Quantitative biochronology of Pliocene and early Pleistocene calcareous nannofossils from the Atlantic, Indian and Pacific oceans. *Mar. Micropaleontol.,* 8:141–170.

Berger, W.H., Yasuda, M.K., Bickert, T., Wefer, G., and Takayama, T., 1994. Quaternary time scale for the Ontong Java Plateau: Milankovitch template for Ocean Drilling Program Site 806. *Geology,* 22:463–467.

Berggren, W.A., 1969. Paleogene biostratigraphy and planktonic foraminifera of Northern Europe. *Proc. First Int. Conf. Planktonic Microfossils, Geneva, 1967:* Leiden (E.J. Brill), 1:121–160.

Berggren, W.A., Kent, D.V., Swisher, C.C., III, and Aubry, M.-P., 1995. A revised Cenozoic geochronology and chronostratigraphy. *In* Berggren, W.A., Kent, D.V., and Hardenbol, J. (Eds.), *Geochronology, Time Scales and Global Stratigraphic Correlation: A Unified Temporal Framework for an Historical Geology.* Spec. Publ.—Soc. Econ. Paleontol. Mineral., 54:129–212.

Berggren, W.A., Kent, D.V., and van Couvering, J., 1985a. Jurassic to Paleogene: Part 2. Paleogene geochronology and chronostratigraphy. *In* Snelling, N.J. (Ed.), *The Chronology of the Geological Record.* Mem. Geol. Soc. London Mem., 10:141–195.

————, 1985b. The Neogene: Part 2. Neogene geochronology and chronostratigraphy. *In* Snelling, N.J. (Ed.), *The Chronology of the Geological Record.* Mem. Geol. Soc. London, 10:211–260.

Berggren, W.A., and Miller, K.G., 1988. Paleogene tropical planktonic foraminiferal biostratigraphy and magnetobiochronology. *Micropaleontology,* 34:362–380.

Berggren, W.A., and van Couvering, J.A., 1974. The Late Neogene. Biostratigraphy, geochronology and paleoclimatology of the last 15 million years in marine and continental sequences. *Palaeogeogr., Palaeoclimatol,. Palaeoecol.,* 16:1–216.

Blow, W.H., 1969. Late middle Eocene to Recent planktonic foraminiferal biostratigraphy. *In* Brönnimann, P., and Renz, H.H. (Eds.), *Proc. First Int. Conf. Planktonic Microfossils, Geneva, 1967:* Leiden (E.J. Brill), 1:199–422.

————, 1979. *The Cainozoic Globigerinida:* Leiden (E.J. Brill).

Bolli, H.M., and Premoli Silva, I., 1973. Oligocene to Recent planktonic foraminifera and stratigraphy of the Leg 15 sites in the Caribbean Sea. *In* Edgar, N.T., Saunders, J.B., et al., *Init. Repts. DSDP,* 15: Washington (U.S. Govt. Printing Office), 475–497.

Bolli, H.M., and Saunders, J.B., 1985. Oligocene to Holocene low latitude planktonic foraminifera. *In* Bolli, H.M., Saunders, J.B., and Perch-Nielsen, K. (Eds.), *Plankton Stratigraphy:* Cambridge (Cambridge Univ. Press), 155–262.

Borehole Research Group, 1994. *Wireline Logging Services Guide:* Palisades, NY (Lamont-Doherty Earth Observatory, Columbia Univ.).

Bowland, C.L., 1993. Depositional history of the western Colombian Basin, Caribbean Sea, revealed by seismic stratigraphy. *Geol. Soc. Am. Bull.,* 105:1321–1345.

Bowland, C.L., and Rosencrantz, E., 1988. Upper crustal structure of the western Colombian Basin, Caribbean Sea. *Geol. Soc. Am. Bull.,* 100:534–546.

Boyce, R.E., 1976. Definitions and laboratory techniques of compressional sound velocity parameters and wet-water content, wet-bulk density, and porosity parameters by gravimetric and gamma-ray attenuation techniques. *In* Schlanger, S.O., Jackson, E.D., et al., *Init. Repts. DSDP,* 33: Washington (U.S. Govt. Printing Office), 931–958.

————, 1977. Deep Sea Drilling Project procedures for shear strength measurement of clayey sediment using modified Wykeham Farrance laboratory vane apparatus. *In* Barker, P.F., Dalziel, I.W.D., et al., *Init. Repts. DSDP,* 36: Washington (U.S. Govt. Printing Office), 1059–1068.

Bralower, T.J., Leckie, R.M., Sliter, W.V., and Thierstein, H.R., 1995. An integrated Cretaceous microfossil biostratigraphy. *In* Berggren, W.A., Kent, D.V., and Hardenbol, J. (Eds.), *Geochronology, Time Scales and Global Stratigraphic Correlations: A Unified Temporal Framework for an Historical Geology,* Spec. Publ.—Soc. Econ. Paleont. Min., 54:65–79.

Bralower, T.J., and Siesser, W.G., 1992. Cretaceous calcareous nannofossil biostratigraphy of Sites 761, 762, and 763, Exmouth and Wombat Plateaus, northwest Australia. *In* von Rad, U., Haq, B.U., et al., *Proc. ODP, Sci. Results,* 122: College Station, TX (Ocean Drilling Program), 529–556.

Bukry, D., 1973. Low-latitude coccolith biostratigraphic zonation. *In* Edgar, N.T., Saunders, J.B., et al., *Init. Repts. DSDP,* 15: Washington (U.S. Govt. Printing Office), 685–703.

————, 1975. Coccolith and silicoflagellate stratigraphy, northwestern Pacific Ocean, Deep Sea Drilling Project Leg 32. *In* Larson, R.L., Moberly, R., et al., *Init. Repts. DSDP,* 32: Washington (U.S. Govt. Printing Office), 677–701.

Cande, S.C., and Kent, D.V., 1995. Revised calibration of the geomagnetic polarity timescale for the Late Cretaceous and Cenozoic. *J. Geophys. Res.,* 100:6093–6095.

Caron, M., 1985. Cretaceous planktic foraminifera. *In* Bolli, H.M., Saunders, J.B., and Perch-Nielsen, K. (Eds), *Plankton Stratigraphy:* Cambridge (Cambridge Univ. Press), 17–86.

Chaisson, W.P., and Leckie, R.M., 1993. High-resolution Neogene planktonic foraminifer biostratigraphy of Site 806, Ontong Java Plateau (western equatorial Pacific). *In* Berger, W.H., Kroenke, L.W., Mayer, L.A., et al., *Proc. ODP, Sci. Results,* 130: College Station, TX (Ocean Drilling Program), 137–178.

Chaisson, W.P., and Pearson, P.N., in press. Planktonic foraminifer biostratigraphy at Site 925, western tropical Atlantic: the last 12 m.y. *In* Curry, W.B., Shackleton, N.J., Richter, C., Bralower, T.J., et al., *Proc. ODP, Sci. Results,* 154:College Station, TX (Ocean Drilling Program).

Cline, J.D., 1969. Spectrophotometric determination of hydrogen sulfide in natural waters. *Limnol. Oceanogr.,* 14:454–458.

Courtney, R.C., and Mayer, L.A., 1993. Calculating acoustic parameters by a filter correlation method. *J. Acoust. Soc. Am.,* 93:1145–1154.

Curry, W.B., Shackleton, N.J., Richter, C., et al., 1995. *Proc. ODP, Init. Repts.,* 154: College Station, TX (Ocean Drilling Program).

deMenocal, P.B., Bristow, J.F., and Stein, R., 1992. Paleoclimatic applications of downhole logs: Pliocene-Pleistocene results from Hole 798B,

Sea of Japan. *In* Pisciotto, K.A., Ingle, J.C., Jr., von Breymann, M.T., Barron, J., et al., *Proc. ODP, Sci. Results,* 127/128 (Pt. 1): College Station, TX (Ocean Drilling Program), 393–406.

Dewan, J.T., 1983. *Essentials of Modern Open-Hole Log Interpretation:* Tulsa (PennWell).

Diebold, J.B., Driscoll, N., Abrams, L., Buhl, P., Donnelly, T., Laine, E., and Leroy, S., 1995. A regional geophysical survey of the Venezuelan Basin and Beata Ridge: implications for the interpretations of stratigraphy and tectonics. *Eos,* 76:614.

Droxler, A.W., 1995. *Caribbean Drilling Program; R/V Maurice Ewing Site Survey Preliminary Report,* ODP Data Bank: Palisades, NY (Lamont-Doherty Earth Observatory, Columbia Univ.).

Droxler, A.W., Cunningham, A., Hine, A.C., Hallock, P., Duncan, D., Rosencrantz, E., Buffler, R., and Robinson, E., 1992. Late middle (?) Miocene segmentation of an Eocene–early Miocene carbonate megabank on the Northern Nicaragua Rise tied to the tectonic activity at the North America/Caribbean Plate Boundary Zone. *Eos,* 73:299.

Droxler, A.W., Cunningham, A.D., Mucciarone, D., and Rosencrantz, E., 1995. Imaging the Hess Escarpment by Hydrosweep, high-resolution seismic, and magnetism, northeast Columbian Basin, Caribbean Sea. *Geol. Soc. Am. Abstr. Prog.,* New Orleans. (Abstract)

Ekstrom, M.P., Dahan, C.A., Chen, M.-Y., Lloyd, P.M., and Rossi, D.J., 1986. Formation imaging with microelectrical scanning arrays. *Trans. SPWLA 27th Annu. Logging Symp.,* Pap. BB.

Ellis, D.V., 1987. *Well Logging for Earth Scientists:* Amsterdam (Elsevier).

Emeis, K.-C., and Kvenvolden, K.A., 1986. Shipboard organic geochemistry on *JOIDES Resolution. ODP Tech. Note,* 7.

Erba, E., Premoli Silva, I., and Watkins, D.K., 1995. Cretaceous calcareous plankton biostratigraphy of Sites 872 through 879. *In* Haggerty, J.A., Premoli Silva, I., Rack, F., and McNutt, M.K. (Eds.), *Proc. ODP, Sci. Results,* 144: College Station, TX (Ocean Drilling Program), 157–169.

Espitalié, J., Deroo, G., and Marquis, F., 1986. La pyrolyse Rock-Eval et ses applications, Partie III. *Rev. Inst. Fr. Pet.,* 41:73–89.

Fisher, R.V., and Schmincke, H.-U., 1984. *Pyroclastic Rocks:* New York (Springer-Verlag).

Gieskes, J.M., Gamo, T., and Brumsack, H., 1991. Chemical methods for interstitial water analysis aboard *JOIDES Resolution. ODP Tech. Note,* 15.

Govindaraju, K., 1989. 1989 compilation of working values and sample description for 272 geostandards. *Geostand. Newsl.,* 13 (spec. iss.).

Gradstein, F.M., Agterberg, F.P., Ogg, J.G., Hardenbol, J., van Veen, P., Thierry, J., and Huang, Z., 1994. A Mesozoic time scale. *J. Geophys. Res.,* 99:24051–24074.

Grau, J.A., and Schweitzer, J.S., 1989. Elemental concentrations from thermal neutron capture gamma-ray spectra in geological formations. *Nucl. Geophys.,* 3:1–9.

Grau, J.A., Schweitzer, J.S., and Hertzog, R.C., 1990. Statistical uncertainties of elemental concentrations extracted from neutron-induced gamma-ray measurements. *IEEE Trans. Nucl. Sci.,* 37:2175–2178.

Hertzog, R.C., Colson, J.L., Seeman, B., O'Brien, M., Scott, H., McKeon, D., Wraight, P., Grau, J., Ellis, D., Schweitzer, J., and Herron, M., 1987. Geochemical logging and spectrometry tools. *Soc. Pet. Eng., Spec. Pap.,* 16792:447–460.

————, 1989. Geochemical logging with spectrometry tools. *SPE Form. Eval.,* 4:153–162.

Hilgen, F.J., 1991a. Astronomical calibration of Gauss to Matuyama sapropels in the Mediterranean and implication for the geomagnetic polarity time scale. *Earth Planet. Sci. Lett.,* 104:226–244.

————, 1991b. Extension of the astronomically calibrated (polarity) time scale to the Miocene/Pliocene boundary. *Earth Planet. Sci. Lett.,* 107:349–368.

Hoppie, B.W., Blum, P., and the Shipboard Scientific Party, 1994. Natural gamma-ray measurements on ODP cores: introduction to procedures with examples from Leg 150. *In* Mountain, G.S., Miller, K.G., Blum, P., et al., *Proc. ODP, Init. Repts.,* 150: College Station, TX (Ocean Drilling Program), 51–59.

Jochum, K.P., Seufert, H.M., and Thirlwall, M.F., 1990. High-sensitivity Nb analysis by spark-source mass spectrometry (SSMS) and calibration of XRF Nb and Zr. *Chem. Geol.,* 81:1–16.

Kameo, K., Sato, T., and Takayama, T., 1995. Late Pliocene calcareous nannofossil datums and biohorizons. *In* Flores, J.A., and Sierro, F.J., *Proc. 5th Conf. Int. Nannoplankton Assoc., 1993:* Salamanca (Universidad de Salamanca), 87–98.

Kennett, J.P., and Srinivasan, M.S., 1983. *Neogene Planktonic Foraminifera: A Phylogenetic Atlas:* Stroudsburg, PA (Hutchinson Ross).

Le Bas, M., Le Maitre, R.W., Streckeisen, A., and Zanettin, B., 1986. A chemical classification of volcanic rocks based on the total alkali-silica diagram. *J. Petrol.,* 27:745–750.

Leckie, R.M., Farnham, C., and Schmidt, M.G., 1993. Oligocene planktonic foraminifer biostratigraphy of Hole 803D (Ontong Java Plateau) and Hole 628A (Little Bahama Bank), and comparison with the southern high latitudes. *In* Berger, W.H., Kroenke, L.W., Mayer, L.A., et al., *Proc. ODP, Sci. Results,* 130: College Station, TX (Ocean Drilling Program), 113–136.

Lock, G.A., and Hoyer, W.A., 1971. Natural gamma-ray spectral logging. *Log Analyst,* 12:3–9.

MacKenzie, W.S., Donaldson, C.H., and Guilford, C., 1982. *Atlas of Igneous Rocks and their Textures:* Harlow, England (Longman).

Manheim, F.T., and Sayles, F.L., 1974. Composition and origin of interstitial waters of marine sediments, based on deep sea drill cores. *In* Goldberg, E.D. (Ed.), *The Sea* (Vol. 5): *Marine Chemistry: The Sedimentary Cycle:* New York (Wiley), 527–568.

Mayer, L.A., Courtney, R.C., and Moran, K., 1987. Ultrasonic measurements of marine sediment properties. *Proc. Oceanogr.,* 87:1–139.

Mazzullo, J.M., Meyer, A., and Kidd, R.B., 1988. New sediment classification scheme for the Ocean Drilling Program. *In* Mazzullo, J., and Graham, A.G. (Eds.), *Handbook for Shipboard Sedimentologists.* ODP Tech. Note, 8:45–67.

McKee, E.D., and Weir, G.W., 1953. Terminology for stratification and cross-stratification in sedimentary rocks. *Geol. Soc. Am. Bull.,* 64:381–390.

Monechi, S., and Thierstein, H.R., 1985. Late Cretaceous-Eocene nannofossil and magnetostratigraphic correlations near Gubbio, Italy. *Mar. Micropaleontol.,* 9: 419–440.

Nederbragt, A.J., 1991. Late Cretaceous biostratigraphy and development of Heterohelicidae planktic foraminifera. *Micropaleontology,* 37:329–372.

Norrish, K., and Chappell, B., 1977. X-ray fluorescence spectrometry. *In* Zussman, J. (Ed.), *Physical Methods in Determinative Mineralogy:* New York (Academic Press), 201–272.

Norrish, K., and Hutton, J.T., 1969. An accurate X-ray spectrographic method for the analysis of a wide range of geological samples. *Geochim. Cosmochim. Acta,* 33:431–453.

Okada, H., and Bukry, D., 1980. Supplementary modification and introduction of code numbers to the low-latitude coccolith biostratigraphic zonation (Bukry, 1973; 1975). *Mar. Micropaleontol.,* 5:321–325.

Olafsson, G., 1991. Quantitative calcareous nannofossil biostratigraphy and biochronology of early through late Miocene sediments from DSDP Hole 608. *Medd. Stockholm Univ. Inst. Geol. Geochem.,* 203.

Paleogene Working Group on Planktonic Foraminifera, in press. *Atlas of Paleocene Planktonic Foraminifera.*

Pearson, P.N., and Chaisson, W.P., in press. Planktonic foraminifer stratigraphy at Ceara Rise, middle Miocene to Paleocene. *In* Shackleton, N.J., Curry, W.B., Richter, C., and Bralower, T.J. (Eds.), *Proc. ODP, Sci. Results,* 154: College Station, TX (Ocean Drilling Program).

Perch-Nielsen, K., 1985a. Cenozoic calcareous nannofossils. *In* Bolli, H.M., Saunders, J.B., and Perch-Nielsen, K. (Eds.), *Plankton Stratigraphy:* Cambridge (Cambridge Univ. Press), 427–554.

————, 1985b. Mesozoic calcareous nannofossils. *In* Bolli, H.M., Saunders, J.B., and Perch-Nielsen, K. (Eds.), *Plankton Stratigraphy:* Cambridge (Cambridge Univ. Press), 329–426.

Peters, K.E., 1986. Guidelines for evaluating petroleum source rock using programmed pyrolysis. *AAPG Bull.,* 70:318–329.

Postuma, J.A., 1971. *Manual of Planktonic Foraminifera:* London (Elsevier).

Pozzi, J-P., Barthes V., Thibal J., Pocachard J., Lim M., Thomas T., and Pages G., 1993. Downhole magnetostratigraphy in sediments: comparison with the paleomagnetism of a core. *J. Geoph. Res.,* 98:7939–7957.

Pozzi, J.-P., Martin, J.P., Pocachard, J., Feinberg, H., and Galdeano, A., 1988. In situ magnetostratigraphy: interpretation of magnetic logging in sediments. *Earth Planet. Sci. Lett.,* 88:357–373.

Premoli Silva, I., and Sliter, W.V., 1994. Cretaceous planktonic foraminiferal biostratigraphy and evolutionary trends from the Bottaccione Section, Gubbio, Italy. *Palaeontogr. Ital.,* 82:2–90.

Premoli Silva, I., and Spezzaferri, S., 1990. Paleogene planktonic forminifer biostratigraphy and paleoenvironmental remarks on Paleogene sediments from Indian Ocean sites, Leg 115. *In* Duncan, R.A., Backman, J., Peter-

son, L.C., et al., *Proc. ODP, Sci. Results,* 115: College Station, TX (Ocean Drilling Program), 277–314.

Raffi, I., and Flores, J.-A., 1995. Pleistocene through Miocene calcareous nannofossils from eastern equatorial Pacific Ocean (Leg 138). *In* Pisias, N.G., Mayer, L.A., Janecek, T.R., Palmer-Julson, A., and van Andel, T.H. (Eds.), *Proc. ODP, Sci. Results,* 138: College Station, TX (Ocean Drilling Program), 233–286.

Ratcliffe, E.H., 1960, The thermal conductivities of ocean sediments. *J. Geophys. Res.,* 65:535–1541.

Reynolds, R.C., Jr., 1963. Matrix corrections in trace element analysis by X-ray fluorescence: estimation of the mass absorption coefficient by Compton scattering. *Am. Mineral.,* 48:1133–1143.

———, 1967. Estimation of mass absorption coefficients by Compton scattering: improvements and extensions of the method. *Am. Mineral.,* 52:1493–1502.

Robaszynski, F., and Caron, M. (Coord.), 1979. Atlas of mid-Cretaceous planktonic foraminifera (Boreal Sea and Tethys). *Cah. Micropaleontol.*

Robaszynski, F., Caron, M., Gonzales-Donoso, J.-M., Wonders, A.A.H., and the European Working Group on Planktonic Foraminifera, 1984. Atlas of Late Cretaceous globotruncanids. *Rev. Micropaleontol.,* 26:145–305.

Ruckebusch, G., 1983. A Kalman filtering approach to natural gamma ray spectroscopy in well logging. *IEEE Trans. Autom. Control,* AC-28:372–380.

Sato, T., Kameo, K., and Takayama, T., 1991. Coccolith biostratigraphy of the Arabian Sea. *In* Prell, W.L., Niitsuma, N., et al., *Proc. ODP, Sci. Results,* 117: College Station, TX (Ocean Drilling Program), 37–54.

Schlager, W., and James, N.P., 1978. Low-magnesian calcite limestones forming at the deep-sea floor, Tongue of the Ocean, Bahamas. *Sedimentology,* 25:675–702.

Schlumberger, 1989. *Log Interpretation Principles/Applications:* Houston, TX (Schlumberger Educ. Services).

Schweitzer, J.S., Grau, J.A., and Hertzog, R.C., 1988. Precision and accuracy of short-lived activation measurements for in situ geological analyses. *J. Trace Microprobe Techniques,* 6:437–451.

Scott, H.D., and Smith, M.P., 1973. The aluminum activation log. *Log Analyst,* 14:3–12.

Shackleton, N.J., Berger, A., and Peltier, W.A., 1990. An alternative astronomical calibration of the lower Pleistocene timescale based on ODP Site 677. *Trans. R. Soc. Edinburgh: Earth Sci.,* 81:251–261.

Shackleton, N.J., Crowhurst, S., Hagelberg, T., Pisias, N.G., and Schneider, D.A., 1995. A new late Neogene time scale: application to Leg 138 sites. *In* Pisias, N.G., Mayer, L.A., Janecek, T.R., Palmer-Julson, A., and van Andel, T.H. (Eds.), *Proc. ODP, Sci. Results,* 138: College Station, TX (Ocean Drilling Program), 73–101.

Shipboard Scientific Party, 1994. Explanatory notes. *In* Mountain, G.S., Miller, K.G., Blum, P., et al., *Proc. ODP, Init. Repts.,* 150; College Station, TX (Ocean Drilling Program), 21–42.

———, 1995. Explanatory notes. *In* Curry, W.B., Shackleton, N.J., Richter, C., et al., *Proc. ODP, Init. Repts.,* 154: College Station, TX (Ocean Drilling Program), 11–38.

———, 1996. Explanatory notes. *In* Paull, C.K., Matsumoto, R., Wallace, P.J., et al., *Proc. ODP, Init. Repts.,* 164: College Station, TX (Ocean Drilling Program), 13–41.

Sigal, J., 1977. Essai de zonation du Crétacé méditerranéen à l'aide des foraminifères planctoniques. *Geol. Mediterr.,* 4:99–108.

Sissingh, W., 1977. Biostratigraphy of Cretaceous calcareous nannoplankton. *Geol. Mijnbouw,* 56:37–50.

Smit, J., 1982. Extinction and evolution of planktonic foraminifera after a major impact at the Cretaceous/Tertiary boundary. *In* Silver, L.T., and Schultz, H. (Eds.), *Geological Implications of Impacts of Large Asteroids and Comets on the Earth.* Spec. Pap. Geol. Soc. Am., 190:329–352.

Spezzaferri, S., and Premoli Silva, I., 1991. Oligocene planktonic foraminiferal biostratigraphy and paleoclimatic interpretation from Hole 538A, DSDP Leg 77, Gulf of Mexico. *Palaeogeogr., Palaeoclimatol., Palaeoecol.,* 83:217–263.

Takayama, T., 1993. Notes on Neogene calcareous nannofossil biostratigraphy of the Ontong Java Plateau and size variations of *Reticulofenestra* coccoliths. *In* Berger, W.H., Kroenke, L.W., Mayer, L.A., et al., *Proc. ODP, Sci. Results,* 130: College Station, TX (Ocean Drilling Program), 179–229.

Takayama, T., and Sato, T., 1987. Coccolith biostratigraphy of the North Atlantic Ocean, Deep Sea Drilling Project Leg 94. *In* Ruddiman, W.F., Kidd, R.B., Thomas, E., et al., *Init. Repts. DSDP,* 94 (Pt. 2): Washington (U.S. Govt. Printing Office), 651–702.

Thierstein, H.R., Geitzenauer, K., Molfino, B., and Shackleton, N.J., 1977. Global synchroneity of late Quaternary coccolith datum levels: validation by oxygen isotopes. *Geology,* 5:400–404.

Timur, A., and Toksöz, M.N., 1985. Downhole geophysical logging. *Annu. Rev. Earth Planet. Sci.,* 13:315–344.

Tissot, B.P., and Welte, D.H., 1984. *Petroleum Formation and Occurrence* (2nd ed.): Heidelberg (Springer-Verlag).

Toumarkine, M., and Luterbacher, H., 1985. Paleocene and Eocene planktic foraminifera. *In* Bolli, H.M., Saunders, J.B., and Perch-Nielsen, K. (Eds.), *Plankton Stratigraphy:* Cambridge (Cambridge Univ. Press), 87–154.

Von Herzen, R.P., and Maxwell, A.E., 1959. The measurement of thermal conductivity of deep-sea sediments by a needle-probe method. *J. Geophys. Res.,* 64:1557–1563.

Walker, D., 1973. Behavior of X-ray mass absorption coefficients near absorption edges: Reynold's method revisited. *Am. Mineral.,* 58:1069–1072.

Wei, W., 1993. Calibration of upper Pliocene–lower Pleistocene nannofossil events with oxygen isotope stratigraphy. *Paleoceanography,* 8:85–99.

Wessel, P., and Smith, W.H.F., 1991. Free software helps map and display data. *Eos,* 72:441, 445–446.

Ms 165IR-102